THE IDH-TAU-EGFR TRIAD DEFINES THE NEOVASCULAR LANDSCAPE OF DIFFUSE GLIOMAS

Gargini R, Segura-Collar B, Herránz B, García-Escudero V, Romero-Bravo A, Núñez FJ, García-Pérez D, Gutiérrez-Guamán J, Ayuso-Sacido A, Seoane J, Pérez-Núñez A, Sepúlveda-Sánchez JM, Hernández-Laín A, Castro MG, García-Escudero R, Ávila J, Sánchez-Gómez P. The IDH-TAU-EGFR triad defines the neovascular landscape of diffuse gliomas. Sci Transl Med. 2020 Jan 22;12(527):eaax1501. doi: 10.1126/scitranslmed.aax1501. PMID: 31969485; PMCID: PMC7055928.

Title: IDH-Tau-EGFR triad defines the neovascular landscape of diffuse gliomas by controlling mesenchymal differentiation

Running title: Glioma genotype defines the vascular phenotype

Ricardo Gargini[1,2*], Berta Segura-Collar[2*], Beatriz Herránz[2,4], Vega Garcia-Escudero[1,3], Andrés Romero-Bravo[2], Felipe J Núñez[5], Daniel García-Pérez[6], Jacqueline Gutiérrez-Guamán[7], Angel Ayuso-Sacido[8,9,10], Joan Seoane[11,12,13], Angel Pérez-Núñez[6], Juan M. Sepúlveda-Sánchez[7], Aurelio Hernández-Laín[7], María G. Castro[5], Ramón García-Escudero[7,12,14], Jesús Ávila[1,15†] and Pilar Sánchez-Gómez[2†#].

[1]Centro de Biología Molecular "Severo Ochoa" (CSIC-UAM), Madrid, Spain;

[2]Neurooncology Unit, Instituto de Salud Carlos III-UFIEC, Madrid, Spain;

[3]Dto. de Anatomía, Histología y Neurociencia; Facultad de Medicina de la Universidad Autónoma, Madrid, Spain;

[4]Facultad de Medicina de la Universidad Francisco de Vitoria, Madrid, Spain

[5]Department of Neurosurgery/Department of Cell & Developmental Biology, The University of Michigan School of Medicine, Ann Arbor, MI, USA.

[6]Dto. Neurocirugía, Hospital 12 de Octubre, Univ. Complutense, Madrid, Spain

[7]Instituto de investigaciones Biomédicas I+12, Hosp. 12 de Octubre, Madrid, Spain

[8]Fundación de Investigación HM Hospitales, HM Hospitales, Madrid, Spain;

[9]Facultad de Medicina (IMMA), Universidad San Pablo-CEU, Madrid, Spain;

[10]IMDEA Nanoscience, Madrid, Spain.

[11]Vall d'Hebron Institute of Oncology (VHIO), Barcelona, Spain;

[12]Centro de Investigación Biomédica en Red de Cáncer (CIBERONC), Spain;

[13]Institució Catalana de Recerca i Estudis Avançats (ICREA), Barcelona, Spain.

[14]Unidad de Oncología Molecular, CIEMAT, Madrid, Spain.

[15]Centro de Investigación Biomédica en Red sobre Enfermedades Neurodegenerativas (CIBERNED), ISCIII, Spain

* Equal contribution

Lead Contact

†Correspondence to: **psanchez@isciii.es**, Dr. Pilar Sanchez-Gomez, Neurooncology Unit, Instituto de Salud Carlos III-UFIEC, Madrid, Spain, Crtra/ Majadahonda-Pozuelo, Km 2, Majadahonda, 28220, Spain. Phone: 34918223265; Fax: 34918223269

†Correspondence to: **jesus.avila@csic.es**, Prof. Jesús Ávila, Department of Neurobiology, Centro de Biología Molecular Severo Ochoa, Cantoblanco 28049, C/Nicolás Cabrera 1, 28049 Madrid, Spain; Tel: + 34 91 1964564

One Sentence Summary

Tau, which is induced by IDH mutations, inhibits the EGFR/NF-kB/TAZ axis and impairs the mesenchymal/pericyte-like transformation of glioma cells, normalizing the vasculature and impairing tumor aggressiveness.

Abstract

Mutant IDH1/2 gliomas represent a more indolent form of cancer. However, how this group of tumors evolve, in a microenvironment-dependent manner, is still a pending question. Here we describe that the expression of *Tau*, a gene classically associated with neurodegenerative diseases, is epigenetically controlled by the balance between wild-type and mutant IDH1/2 in gliomas. Moreover, the amount of *Tau* decreases when the tumor progresses. Besides, Tau is almost absent from tumors with EGFR mutations, whereas its trancription is inversely correlated with overall survival in gliomas carrying wild-type or amplified EGFR. We demonstrate that the overexpression of Tau, through the stabilization of microtubules, impairs the mesenchymal/pericyte-like transformation of glioma cells by blocking the EGFR-NFκB-TAZ axis. However, mutant EGFR induces a constitutive activation of this pathway, which is no longer sensitive to Tau. By inhibiting the phenotypic plasticity of EGFRamp/wt glioma cells, Tau protein inhibits angiogenesis and favors vascular normalization, decreasing tumor aggressiveness and rendering the tumors more sensitive to chemotherapy.

Keywords: Glioma; Tau (MAPT); IDH1/2 mutations; EGFR; microtubule stabilizers; TAZ; NF-kB; Cancer-Stem-Cell (CSC) plasticity; epithelial-to-mesenchymal (EMT) transition; tumor-derived-pericytes, vascular normalization; tumor-microenvironment (TME)

Words: 9999
Figures: 8
Pages: 26

INTRODUCTION

Diffuse gliomas are classified and graded according to histological criteria. They include low and intermediate-grade gliomas (herein called Lower-Grade Gliomas, LGG), which encompass World Health Organization (WHO) grades 2 and 3, and the highly aggressive WHO grade 4 glioblastomas (GBM), with 5-year survival rates of 5%. They are categorized based on the increments in cellular atypia and mitotic activity. On top of that, GBM are characterized by the specific presence of areas of necrosis and robust neoangiogenesis, being considered one of the most vascularized cancers. LGG are more indolent tumors although many of them progress into secondary GBM, albeit at highly variable intervals, with survival rates that goes from 1 to 15 years (1). Unfortunately, little is known about the factors that drive this transition from LGG to GBM.

A big effort has been made in the last two decades in order to characterize the genetic modifications associated with gliomas. Some of them have been incorporated into the novel WHO classification. Particularly, the identification of mutations in the *IDH1/2* (*Isocitrate dehydrogenase 1/2*) genes, which are associated with a more favorable prognosis in gliomas (2), is common now in the routine clinical practice. IDH1/2 mutated proteins induce the accumulation of the oncometabolite, 2-D-hydroxyglutarate (2-HG), which competes with the α-ketoglutarate (α-KG) produced by the wild-type IDH enzymes and blocks TET (Ten Eleven Translocation)-mediated DNA demethylation. This process generates a CpG island methylator phenotype (G-CIMP), which is associated with a general suppression of gene expression (3). Moreover, 2-HG inhibits histone demethylases, which further contribute to this phenotype (4). By contrast, wild-type IDH1 promotes the metabolic adaptation of GBM cells to support aggressive growth (5). Therefore, it has been proposed that the balance between wild-type and mutant IDH1/2 function determines the clinical outcome of gliomas, including their sensitivity to radiation and chemotherapy (6).

Within the new subclasses of high grade gliomas (proneural (PN), classic (CL) or mesenchymal (MES)), *IDH1/2* mutations are accumulated in the first group, which is enriched in secondary GBM and includes tumors with a better clinical prognosis (7). By contrast, mutations in *EGFR* (Epidermal growth factor receptor) accumulate in the CL and MES subtypes. This gene is mutated and/or amplified in a large percentage of diffuse gliomas and it has been associated with proliferation and survival, as well as with the invasive properties of glioma cells (7;8).

Several cytoskeletal proteins have been involved in tumor progression. Tau, encoded by the gene *MAPT* (Microtubule-associated protein tau), is well-known for its relevance in Alzheimer´s disease (AD) although it is also expressed in healthy brains, where it controls neural development and synaptic transmission (9). In addition, Tau and

other microtubule-stabilizing agents like taxanes modulate protein and organelle trafficking (10;11), which could be relevant for cancer cells. Interestingly, a possible co-morbidity of dementias and GBM had been suggested (12), which led us to perform a bioinformatic analysis. We found that *Tau (MAPT)*, among other genes related to neurodegeneration, is expressed in gliomas, where it seems to correlate negatively with tumor progression (13). Based on these data, we decided to conduct a more comprehensive characterization of Tau in this deadly pathology. Here we show that the expression of this protein depends on the genetic status of *IDH1/2*, being enriched in LGG and PN gliomas, where it hinders tumor progression. Mechanistically, Tau inhibits the EGFR-NF-kB-TAZ signaling pathway, provided that no EGFR mutations are present. By blocking this cascade, it impedes the plasticity of the tumor cells and their capacity to generate mesenchymal/pericyte-like cells, which participate in the processes of angiogenesis and neo-vascularization. As a consequence, Tau favors the normalization of the glioma´s vasculature and hampers tumor progression.

RESULTS

High expression of Tau (MAPT) correlates inversely with glioma aggressiveness

The in silico analysis of the glioma TCGA data set showed that the quantity of *Tau (MAPT)* decreases as the tumor grade increases, at least in astrocytomas (Fig. 1A, and fig. S1 A and B). Moreover, a higher transcription of this gene was associated with an increased overall survival of glioma patients (Fig. 1B and C, fig S1C to F). These results confirmed our previous data (13) and prompted us to perform an immunohistochemical (IHC) staining on glioma samples, which showed that Tau protein is clearly expressed in the cytoplasm of tumor cells, with a very different pattern to the one observed in normal tissue (NT) (Fig. 1D, and fig. S1G). Besides, we found a high amount of Tau in a subset of the gliomas analyzed by Western Blot (WB) (Fig. 1E). The quantification of the IHC staining (Fig. 1F) and the WB (Fig. 1G) confirmed that Tau protein is clearly enriched in LGG compared to GBM. Although this accumulation could explain by itself the survival data, we found that the transcription of Tau correlates with an increased overall survival in separated GBM (Fig. 2A) and LGG (Fig. 2B) cohorts. Similar results were obtained when we measured *Tau* by qRT-PCR analysis in our own GBM cohort (Fig. 2C). Collectively, these results support the idea that this gene is associated with a less aggressive behavior of gliomas, independently of the tumor grade. Furthermore, we found a marked decrease in the expression of *Tau* in disease free vs progressed tumors (Fig. 2D). To confirm these observations we performed a longitudinal IHC quantification of Tau in primary LGG and their recurrent paired samples. Remarkably, we found a

consistent reduction of Tau in those tumors that had progress into a more aggressive phenotype (Fig. 2E), which was not observed when there was no change in the histological classification of the recidives (Fig. 2F). These results suggest that Tau downregulation must be important for the tumors to relapse after surgical resection, which is a critical step in the mortality related to this pathology.

To further asses the presence of Tau in glioma cells and its participation in tumor aggressiveness we analyzed its expression in a panel of patient-derived-xenografts (PDX), obtained from GBM surgeries and grown subcutaneously, devoided of any trapped neurons. As we had previously observed in tumor samples (Fig. 1E), the quantity of Tau protein in the PDXs was highly variable (Fig. 2G, and fig. S2A). It is important to remark that in the Tau-high tumors, a big percentage of GFAP cells were positive for Tau staining (fig S2A and fig. S2B), further supporting the specific presence of this protein in glioma cells.

In order to know if the amount of Tau affects tumor behavior, we injected some of the PDX cells into the brains of immunodeficient mice. We observed a decrease in tumor burden (Fig. 2H) after the injection of Tau-high primary cell lines (measured by qRT-PCR with human specific primers (Fig. 2I)). Moreover, the overexpression of this gene in a Tau-deficient glioma cell line (12o15) delayed tumor formation (Fig. 2J and fig. S2C), whereas its downregulation in Tau-enriched cells (12o02) clearly increased their aggressive behavior (Fig. 2K and fig. S2D). Altogether, our results confirm the presence of Tau in the tumor cells of several gliomas, especially in the less aggressive ones. Additionally, they suggest that this protein could be playing an active role as an inhibitor of tumor progression.

The expression of Tau (MAPT) in gliomas is regulated by IDH function

We analyzed the genetic background of gliomas in relation to the quantity of *Tau (MAPT)* and we found that *IDH1* mutations accumulate in Tau-high gliomas (Fig. 3A). This correlation was validated using a Volcano Plot analysis (Fig. 3B). Furthermore, Tau protein was detected in the majority of tumor cells that express the most common IDH1 mutation (R132H) (fig. S3A and B), further confirming that the protein is truly expressed in the tumor cells. We then measured Tau IHC staining in wild-type and mutant *IDH* gliomas and we found a clear enrichment of high and medium stained sections in the second group (Fig. 3C). These results highlight the correlation between the presence of IDH mutations and the expression of Tau, which seems to be independent of the tumor grade as we found a higher amount of *Tau* in *IDH* mutant compared to *IDH* wild-type tumors in the GBM (fig. S3C) and in the LGG (fig. S3D) TCGA cohorts. In order to confirm

this relationship we analyzed a recently published glioma model, in which IDH1 wt or IDH R132H is expressed in an *ATRX* mutant background (14). As expected, there was a clear delay in the tumor growth in the presence of mutant IDH1 (Fig. 3D). Moreover, we measured a clear increase in the quantity of Tau protein in the mutant compared to the wild-type dissected allografts (Fig. 3E), suggesting that the expression of Tau in gliomas is induced by mutant IDH proteins.

The G-CIMP phenotype, which is associated with the presence of *IDH* mutations, is supposed to block the transcription of many genes. However, it also activates certain others, especially those involved in the tumorigenesis of LGG (like the *PDGFRA (Platelet Derived Growth Factor Receptor Alpha)* oncogene) through the disruption of the repressive structure of the CTCF insulator protein (15). Actually, we observed an increased expression of *Tau* in the G-CIMP GBM subtype (fig. S4A), as well as a strong correlation between *Tau (MAPT)* and *PDGFRA* in the TCGA samples (fig. S4B). To test if the Tau promoter could be epigenetically controlled by IDH mutations, we first analyzed the presence of CpG islands in the *Tau (MAPT*) promoter region by using the xena genome browser. We identified three of them in the 5´region of transcription initiation site (fig. S4C), which correlate with the sites previously described (16). Using epigenetic data from the TCGA (LGG cohort) we compared the methylation of the whole promoter region in mutant vs wild-type IDH tumors. We observed an increased methylation in CpG:26 (Fig. 3F, fig. S4D and E) and in some parts of CpG:302 (fig. S4D and E) in the mutant tumors. However, when we analyzed the ChIP-seq data of the CTCF binding to the different clusters, we observed that only the binding to the CpG:26 site was lost in the *IDHmut* tumors (Fig. 3G). Moreover, when we treated primary GB cells with 2-HG we observed a dose-dependent accumulation of its mRNA (Fig. 3H), an effect that was reversed in the presence of azacytidine (AZA) (Fig. 3I). These results allow us to propose that the increase in the methylation of the CpG:26 region, induced by IDH mutant proteins, changes the chromosomal insulator topology and the binding of CTCF to the *Tau* promoter, activating its transcription.

It is well known that *IDH1/2* mutations define a distinct subset of gliomas with a better outcome, whereas the presence of *IDH* wild-type in LGG and GBM defines a subgroup with poorer prognosis (fig. S4F). Interestingly, we found an inverse correlation between the transcription of wild-type *IDH1* and *Tau* on the TCGA (Fig. 3J) and the Rembrandt (Fig. 3K) cohorts, suggesting that IDH wt function might inhibit the expression of the *Tau* promoter.

Tau opposes EGFR signaling in gliomas

To gain insight into the reduction of tumor aggressiveness by Tau we performed a DAVID gene analysis of the pathways co-upregulated with this gene in gliomas. As expected, we found a positive association with microtubule and neurogenic-related processes. However, the other Tau-linked pathways were somehow related to receptor tyrosine kinases signaling (fig. S5A). In addition, our in silico analysis indicated that *IDH* mutations, as well as a higher amount of *Tau*, are mutually exclusive with *EGFR* and *PTEN* mutations (Fig. 3A, and Fig. 4A, and fig. S5B), which was confirmed in a Volcano Plot analysis (Fig. 4B). To interrogate if Tau could be modulating this signaling pathway, we expressed IDH wt or IDH R132H in a EGFR amplified cell line (RG1). As we have previously observed in the mouse glioma model (Fig. 3D), IDH mut impaired tumor burden (Fig. 4C). However, we also observed that the overexpression of IDHwt increases the aggressiveness of the glioma cells (Fig. 4C). These effects were paralleled by changes in the quantity of Tau, which augmented in IDH mut and decreased in IDH wt tumors, compared to the control ones (Fig. 4D and E). This result is in agreement with the in silico data (Fig. 3J an K), and allows us to propose that the induction of Tau transcription might depend on the blance between wild-type and mutant IDH functions. Interestingly, the phosphorylation of EGFR showed a striking inverse correlation with the quantity of Tau in mouse tumors (Fig. 4D and F) and in human samples (fig. S5C and D). More importantly, the expression of *Tau* correlated with overall survival in the group of *EGFR*amp/wt gliomas (Fig. 4G) but it had no clinical relevance in the presence of additional mutations in *EGFR* (Fig. 4H). Taken together, these results highlight that there could be a negative effect of IDH/Tau on the pathway activated by this receptor, but only in the group of *EGFR*amp/wt gliomas.

To evaluate the effect of Tau on EGFR signaling, we overexpressed this protein in two mouse glioma models: SVZ-EGFRamp/wt and SVZ-EGFRvIII, and we analized their capacity to grow as intracranial allografts. These models were generated by transforming subventricular zone (SVZ) progenitors from p16/p19 ko mice with retrovirus expressing either the wild-type or the variant III (vIII) isoform of the receptor. Both type of cells depend on EGFR signaling *in vitro* and *in vivo* and they generate gliomas with a high penetrance. Overexpression of Tau clearly inhibited the growth of SVZ-EGFRamp/wt mouse gliomas (Fig. 4I) but it had no effect on SVZ-EGFRvIII tumors (Fig. 4J). Similar results were obtained when we overexpressed Tau in two human primary cell lines, RG1 (*EGFR*amp) and 12o150 (*EGFR* amplified and mutated, *EGFR*mut). Tau impaired the growth of the first (Fig. 4K) but it had no effect on the second (Fig. 4L). Remarkably, Tau did not inhibit the survival or the self-renewal capacity of the mouse (fig. S5E and F) or the human (fig. S5G and H) glioma cells *in vitro*, suggesting that the

consequence of Tau overexpression on EGFR signaling pathway must be only relevant in the context of the tumor microenvironment (TME).

Microtubule stabilizators like Tau and EpoD favor the degradation of wild-type EGFR

When we analyzed the dissected tumors after Tau overexpression we observed that the amount of phospho-EGFR was attenuated in SVZ-EGFRamp/wt tumors (Fig. 5A) as well as in *EGFR*amp xenografts (Fig. 5B), whereas there was no change in SVZ-EGFRvIII gliomas (Fig. 5C) or in *EGFR*mut xenografts (Fig. 5D). These data reinforce the notion that Tau opposes wild-type but not mutant EGFR signaling.

Previous results from our group have demonstrated that, as a result of Tau function, stabilized microtubules become heavily acetylated through the inhibition of HDAC6 (histone deacetylase 6). In fact, the increase in tubulin acetylation can serve as a readout of Tau expression (17). Moreover, it has been proposed that this acetylation promotes the subsequent degradation of EGFR due to changes in the microtubule-dependent endocytic machinery (18). In agreement with these published data, we observed a higher quantity of acetylated tubulin in Tau overexpressing gliomas, which were paralled by a strong decrease in the amount of total EGFR protein (Fig. 5E). The downregulation of EGFR protein was also observed *in vitro* after Tau overexpression and it was reverted in the presence of MG132 (proteasome inhibitor) or chloroquine (lysosome inhibitor) (Fig. 5F). Therefore, we could propose that Tau impairs EGFR signaling through the stabilization of the microtubules and the subsequent alteration of the receptor trafficking, which leads to its degradation. To validate this hypothesis we treated RG1(*EGFR*amp)-injected mice with a Taxol derivative, Epothilone D (EpoD). This kind of components can also stabilize the microtubules. In fact, they compete with Tau for the same tubulin-binding site. EpoD in particular has been proved to reach the brain and revert some of the axonal defects of a Tau loss-of-function model (19). Systemic treatment with EpoD significantly delayed RG1 tumor formation (Fig. 5G) and reduced phospho-EGFR in the tumors (Fig. 5H and I) without changing the quantity of Tau protein (Fig. 5H). This was accompanied by a strong downregulation of EGFR and a clear increase in the quantity of acetylated tubulin (Fig. 5H and I). Altogether, our data support the notion that the microtubule-related function of Tau is responsible for its effect on EGFR signaling and tumor growth in gliomas. Moreover, they suggest that taxol derivatives could reduce the aggressiviness of gliomas. In fact, we observed that EpoD treatment made RG1 tumors more sensitive to chemotherapy (Fig. 5J), so there could be a therapeutic opportunity for the use of these compounds in glioma patients.

Tau blocks the mesenchymalization of EGFRamp/wt glioma cells.

The bioinformatic analysis showed that *Tau (MAPT)* correlate positively with the PN signature while they exhibit a strong inverse correlation with the MES profile of gliomas (Fig. 6A, and fig. S6A to F). In addition, we observed that *Tau* expression inversely correlates with the NF-κB (Nuclear factor kappa-light-chain-enhancer of activated B cells) and the inflammatory pathways, but not with other signatures, like those associated with hypoxia or PDGFRα (Fig. 6A and B). These in silico observations were confirmed by the WB analysis of RG1 (EGFRamp) xenografts, which showed that overexpression of Tau induces a clear inhibition of the NF-κB subunit phosphorylation, as well as a strong reduction in the amount of TAZ protein, a master regulator of the MES phenotype (20) (Fig. 6C and D). Similar results were obtained in the WB analysis of 12o15 xenografts (Fig. 6E and F), a primary cell line that overexpresses the receptor in the absence of gene amplification (21). However, Tau did not change the transcription of other MES genes (Fig. 6G) and it had no effect on TAZ or NF-κB activation in *EGFR*mut tumors (fig. S6G).

Tau overexpression also induced the transcription of *OLIG2* (Fig. 6H), a gene that is frequently used as a *bona fide* PN marker (22). Moreover, the IF analysis of RG1 gliomas confirmed that Tau represses nuclear TAZ, whereas it induces nuclear OLIG2 in the tumor cells (Fig. 6I). These data were confirmed by RT-PCR analysis of human samples (Fig. 6J and K), and by in silico studies (fig. S6H), which showed that Tau correlates inversely with *TAZ* and positively with *OLIG2* expression. Altogether, our results indicate that Tau induces a change in the glioma phenotype, repressing MES regulators and inducing PN promoters in the tumor cells through the regulation of the EGFR/TAZ/NF-kB pathway. It is important to remark that Tau did not change the tumor burden of RG1 cells in the presence of TAZ overexpression (Fig. 6L and M), which highlights that Tau inhibits the growth of EGFRamp/wt glioma growth by blocking the plasticity of tumor cells and the appearance of mesenchymal features.

Previous results from our group and others have shown that, in comparison with PN cancer stem cells (CSCs), MES CSCs are more capable of glioma initiation, probably associated with their increased angiogenic capacity (23;24). In agreement with this observation, the overexpression of Tau in RG1 cells impaired their capacity to form subcutaneous xenografts (fig. S7A and B). Furthermore, we found that most of the genes upregulated with TAZ in gliomas were associated with angiogenesis and tumor vasculature (fig. S7C to F). Particularly, we noticed that markers of pericytes, which are considered as perivascular MES stem cells (25), were among the genes which correlated better with TAZ in gliomas (fig. S7G and H). In order to examine if this transcription factor

could modulate the function and/or the number of mural cells we expressed shTAZ in RG1 cells and we performed an ortothopic *in vivo* experiment. The knock down of this gene clearly reduced the aggressiviness of the tumors (Fig. 6N) and inhibited the expression of several pericyte markers (Fig. 6O). It is worth mentioning that TAZ seems to regulate peryctic differentiation in a cell-autonomous way as we also observed a reduction of these markers after the *in vitro* lentiviral induction of shTAZ in RG1 and 12o15 cells (Fig. 6P to R). These results are in accordance with some recent publications showing that most of the pericytic functions in GBM are performed by the highly plastic CSCs, which undergo a transdifferentiation process, acquiring mesenchymal and mural cell features (26-28).

Tau reduces the amount of tumor-derived-pericytes and normalizes the vasculature of EGFRamp gliomas

Our results indicate that Tau impairs the mesenchymalization of glioma cells by blocking the expression of TAZ, which is induced in response to EGFR activation. Moreover, we could hypothesize that, as a result of this inhibition, there is an important blockade of the capacity of the tumor cells to transdifferentiate into pericytes. Therefore, we decided to analyze the vascular component of RG1 (EGFRamp) tumors after the overexpression of Tau. We observed a marked decrease in the number of αSMA and CD248 positive cells (Fig. 7A), together with a significant inhibition of the transcription of human pericytic markers, in Tau-expressing tumors (Fig. 7B). A similar result was observed in 12o15 (EGFRwt) (fig. S8A), but not in 12o150 (EGFRmut) xenografts (fig. S8B). Remarkably, Tau did not impaired the transcription of mouse pericityc genes (Fig. 7C), reinforcing the idea that this protein inhibits the glioma-to-pericyte transdifferentiation but it does not influence the quantity and/or the differentiation capacity of host pericytes.

The IF analysis of the tissues also revealed that there was an important inhibition of cellular proliferation (fig. S8C and D) after Tau overexpression, accompanied by a significant decrease in the number of dilated blood vessels (Fig. 7D and E), typical of malignant gliomas (29). The angiogenic signals that are reduced upon Tau induction must be derived, at least in part, from the tumor cells, as the supernatant of RG1 cells overexpressing Tau has a reduced capacity to induce HMBEC (Human Brain Microvascular Endothelial Cells) sprouting (Fig. 7F) and contains less VEGF (Vascular Endothelial Growth Factor) (Fig. 7G).

We had previously noticed the lack of hemorrhages in *EGFR*amp tumors overexpressing Tau, an event that was frequent in control tumors (Fig. 7H). In parallel, we observed a reduction in the extravasation of IgG after Tau induction (Fig. 7I), which indicates that tumors that overexpress Tau present a less aberrant tumor vasculature,

with an increase in the intregrity of the blood brain barrier (BBB). In agreement with this hypothesis, Tau induced a clear reduction in the quantity of Ang2 (Angiopoietin 2) (Fig. 7J), a key regulator of angiogenesis that has been associated with vascular abnormalities in glioma, acting as an antagonist of Ang1 (30). In fact, we observed a significant decrease in the *Ang2/Ang1* ratio after Tau overexpression in the *EGFR*amp model (Fig. 7K), but not in the *EGFR*mut xenografts (fig. S8E). These results suggest that the transdifferentiation of glioma cells into mesenchymal/pericyte-like cells, induced by EGFR signaling, favors the secretion of angiogenic signals and the formation of an aberrant vasculature. This process can be impaired by Tau in EGFRwt/amp, but not in EGFRmut gliomas.

In order to confirm the relevance of the tumor-derived-pericytes in the growth of EGFRamp gliomas, we downregulated *CD248* expression in RG1 cells. CD248 (endosialin) aids in supporting tumor microvasculature and it is expressed in pericytes, especially in malignant solid tumors, including high-grade gliomas (27;31). We picked the most effective shRNA sequences (fig. S8F) and we injected the interfered cells into the brains of immunodeficient mice, in the presence of normal host pericytes. We observed a significant delay in tumor growth after *CD248* downregulation (Fig. 7L). Moreover, the inhibition of *CD248* in the tumor cells reduced the expression of other pericytic markers *in vitro* (fig. S8G) and *in vivo* (Fig. 7M), reinforcing the role of CD248 in the transdifferentiation of tumor cells into pericytes. Furthermore, tumors formed after *CD248* downregulation showed a reduction in the extravasation of IgG (Fig. 7N), as well as a decreased *Ang2/Ang1* ratio (Fig. 7O), which further support the hypothesis that the depletion of tumor-derived-pericytes (at least in EGFRwt/amp tumors) normalizes the glioma vasculature and reduces the aggressiviness of these gliomas.

Tau expression is a surrogate marker of the less aggressive vascular behavior of gliomas

The data presented so far place Tau at the boundary between the most common genetic alterations of gliomas (those that affect *IDH1/2* and *EGFR*) and the regulation of the tumor microenvironment, in particular the vascular phenotype. In order to translate the results into the clinical settings, we used our own cohort of patient´s samples (qRT-PCR analysis) and the data from the TCGA (in silico analysis). We divided the tumors into an IDH1 mut (those with higher transcription of Tau) and an IDH1 wt group, and we subclasified the second one into High or Low-Tau gliomas (Fig. 8A and B). We confirmed the inverse correlation between *Tau* and phospho-EGFR (Fig. 8C) and between the transcription of *CD248* and *Tau* (Fig. 8D and E), which was confirmed by the IHC analysis of the tumors. The representative images in Fig. 8F evidence the gradual normalization

of the vasculature in parallel with the increase in Tau protein (Fig. 8F). Furthermore, the quantification of the CD248 score (Fig. 8G), the transcription of *CD34* (Fig. 8H) and the amount of dilated vessels (Fig. 8I), confirmed the visual differences and reinforced our model, in which Tau expression could function as a surrogate marker of the less aggressive vascular behavior in gliomas.

DISCUSSION

IDH1/2 mutations identify a genetically and clinically distinct glioma entity. Patients with such tumors have a much better prognosis (independently of the histological classification) and they show improved responses to chemotherapy and/or irradiation (32;33). Indeed, the re-expression of IDH1 R132H in GBM cells can reduce tumor growth (Fig. 3D and 4C) (14;34). However, the molecular basis for the tumor-suppressor functions of IDH mutations are unclear. Here, we have identified Tau, a known microtubule stabilizer, as a new epigenetic target of IDHmut in gliomas. Based on our results we can propose that these mutant enzymes, acting through the increase in Tau transcription, favor the normalization of the vasculature and impede the progression of the disease (fig. S9). In fact, Tau downregulation induces a dramatic increase in tumor burden in the orthotopic xenografts. Moreover, the longitudinal analysis of a set of paired samples showed that the quantity of Tau decreases as LGG evolve into higher grade lesions. Interestingly, IDH1/2 status seems to be consistent during glioma progression (35;36), suggesting that some other mechanism is inhibiting Tau transcription in the recurrent tumors. One possible explanation would be that an increase in wild-type IDH protein in the recidives could impair Tau expression, as it happens in the mouse xenografts (Fig. 4D). Indeed, it has been recently shown that the non-mutated IDH1 is upregulated in primary GBM in comparison with secondary GBM or LGG, where it promotes aggressive growth and therapy resistance (5).

From the moment that IDH1/2 mutations were identified in gliomas, it seemed clear that they represent early events in the process of tumorigenesis (37). A decade later we know that these proteins induce important metabolic and epigenomic changes, which could explain their oncogenic properties (4;14;15;38;39). Consequently, a plethora of inhibitors have been developed to block IDHmut function in different cancers. Indeed, some of them have shown anti-tumor acitivty in mouse glioma models (40) and they have been approved to be tested in IDHmut patients (41). However, the tumor-suppressor functions of these proteins in gliomas, including the vascular normalization that we have described here, could represent a severe pitfall for these approaches. In fact, the treatment with IDHmut inhibitors has been associated with a radioprotective effect (42)

and a decreased sensitivity to cisplatin (43). Regarding IDHwt gliomas, our results suggest that microtubule stabilizers could imitate Tau function and reduce the aggressiveness of the tumors, which could render them sensitive to conventional chemotherapy (Fig. 5I). The same compounds could be tested in combination with IDHmut inhibitors in LGG, in an attempt to impair tumor growth and, at the same time, block the transformation into a more aggressive tumors.

Our results indicate that Tau is a key inhibitor of wild-type EGFR signaling in gliomas. Accordingly, drugs that interfere with microtubule function have been associated with EGFR inactivation in other cancers (44), as they seem to alter endocytic trafficking (11). Moreover, it has been shown that microtubule acetylation, which is promoted by Tau function (17), promotes the degradation of EGFR through changes in the microtubule-dependent endocytic trafficking (18). We propose that a similar mechanism could be operating in gliomas, but only in the absence of EGFR mutations. In that sense, EGFR mutant proteins, especially the vIII isoform, has been associated with the maintenance of the signal in the absence of ligands (45), possibly due to changes in the turnover of the mutant receptor (46). Moreover, it has been proposed that some of the EGFR downstream targets, like NF-κB, become constitutively activated in GBM after vIII expression (47). The data presented here further supports that EGFR mutations induce a constitutive activation of NF-κB, which would be unsensitive to microtubule modulators.

Downstream of EGFR/NF-κB signaling, we have found that Tau overexpression severely reduced the amount of TAZ in GBM. TAZ is a transcriptional coactivator that play a prominent role in gliomas (48), controlling the MES signature (20). Moreover, TAZ is induced by NF-κB activation in gliomas and promotes radio-resistance (20). It has been recently proposed that *TAZ* promoter is a direct target of NF-κB (49) so Tau could be inhibiting indirectly the transcription of the *TAZ* gene. However, we cannot discard a possible regulation of the protein stability downstream of EGFR/NF-κB signaling.

It is well known that IDH mutant gliomas are characterized by a lesser extent of contrast enhancement than wild-type tumors, even if we only consider GBM (50). However, the molecular explanation for this behavior was still missing. Our results show that Tau, acting downstream of IDHmut, could normalize the blood vessels and reduce the BBB leakage. These changes could cooperate or even precede other alterations observed in the TME of IDHmut gliomas, like the absence of microthrombi (51), as well as the decrease in necrosis areas (50) and hypoxia-induced angiogenesis (52). Moreover, the immune component and its pro- or anti-tumoral properties could also be affected by the vascular phenotype of IDHmut gliomas (53), explaining the decrease in the immune infiltrate observed in mouse models and human samples (34). Future

experiments are warranted in order to decipher the participation of Tau in these other phenotypes. One limitation of this work is the high intratumoral heterogeneity of gliomas, which express different mutations in a scattered way. Moreover, mixed transcriptomic subpopulations can be found in one single tumor. This could difficult the translation of our homogeneous glioma models into the patients. However, he strong inverse correlation observed in the human samples between Tau and the vascular abnormalities reinforce the implications of our results.

Although cancer and neurodegenerative diseases are considered as opposite phenomena, there could be a positive association between AD prevalence and GBM incidence (12). In AD and other tauopathies, there is an accumulation of Tau aggregates (gain of toxic function). However, this aggregation of Tau compromises its microtubule-stabilising functions (loss of physiological function), favoring the evolution of the pathology. In agreement with the loss-of-function model, we have reported behavioral changes and neurogenesis in aged Tau knockout mice (54). Interestingly, EMT genes are enriched in the affected areas of AD brains (55). Moreover, there is an important neurovascular dysfunction at early stages of AD, associated with BBB breakdown and inflammation (56), which could be linked to pericyte loss (57). Although there is still missing evidence of the relevance of Tau (especially the astrocytic Tau) in these phenotypes, it is tempting to speculate that the loss of function of this protein could represent a link between the progression of the two types of brain diseases. If this hypothesis is correct, targeting pericytes or the mesenchymal transdifferentiation of the astrocytes could be an interesting therapeutic approach to be tested in several neurological disorders. Moreover, it would be worth studying if AD related drugs could be repurposed to treat brain tumors. In that sense, we have demonstrated that EpoD, a microtubule stabilizing agent that reduces AD pathology in mouse models (19), slows down *in vivo* glioma growth without any apparent secondary effect. Another second-generation taxane, cabazitaxel, has demonstrated a good anti-glioma activity in preclinical tests (58) and is being evaluated as a novel cytotoxic therapy (NCT01740570, NCT01866449). However, we propose that lower doses of these compounds could imitate the effect of Tau overexpression, reducing the aggressiviness of gliomas with less secondary effects for the patients. By contrast, as they compete for the same microtubule binding site of Tau, the presence of this protein could identify gliomas that would be resistant to taxol derivatives, as it has been shown for other cancers (59).

Collectively, our results provide and explanation for the better outcome of IDHmut gliomas, which could have important implications for several aspects of glioma research and clinical practice. Moreover, the understanding of how Tau governs the vascular

component of the TME in gliomas could provide novel explanations for the neurovascular dysfunction observed in AD and other dementias.

MATERIALS AND METHODS

Study design

Our overall objective was to characterize the expression and function of Tau in gliomas. For that we used publically available cohorts of human gliomas and samples obtained in the participating hospitals. Moreover, we performed the analysis of Tau overexpression or downregulation in different orthotopic mouse models, including xenografts of human primary cells and mouse glioma allografts. Sample size for those animal experiments was determined before the study as per Institutional Research Ethics and Animal Welfare Committee (CEIyBA) guidelines. Experiments were designed to detect 20% differences between treatment groups or genotype-dependent effects at 80% power ($\alpha = 0.05$). The subjects were not randomly assigned to experimental groups because of animal housing considerations. Treatments were not administered blinded; however, mice were monitored for signs of distress and humane endpoints in a blinded manner. Regarding *in vitro* experiments all the assays were performed with at least triplicate samples. No outliers were excluded. Where possible, studies have been repeated by independent personnel.

Human samples

Glioma tissues (fresh frozen or embedded in paraffin) were obtained after patient´s written consent and with the approval of the Ethical Committees of “Hospital 12 de Octubre” (CEI 14/023) and “Hospitales de Madrid” (14.10.632-GHM, 18.12.1337-GHM) (Table S1 and S2).

Human and mouse glioma cells

RG1 cells were kindly donated by Rosella Galli (San Raffaele Scientific Institute). The rest of the human cells (Table S3) were obtained by dissociation of surgical specimens from patients treated at the “Hospital 12 de Octubre” (Madrid, Spain), after patient´s written consent and with the approval of the Ethical Committee (CEI 14/023). They belong to the Biobank of that Hospital. Cells were grown in Complete Media (CM): Neurobasal supplemented with B27 (1:50) and GlutaMAX (1:100) (Thermo-Fisher-Scientific); penicillin-streptomycin (1:100) (Lonza); 0.4% heparin (Sigma-Aldrich); and 40 ng/ml EGF and 20 ng/ml bFGF2 (Peprotech). Mouse SVZ models were obtained by retroviral expression of EGFRwt or EGFRvIII in primary progenitors from p16/p19 ko mice. These

cells were obtained as previously described (60) and they were grown in CM. After infection, the cells were injected into nude mice and the tumors that grew were dissociated and established as SVZ-EGFRamp/wt or SVZ-EGFRvIII models. Both models express GFP and luciferase as reporters. These cell lines give rise to gliomas when they are implanted (300,000 cells) in the brains of nude mice with a 100% penetrance. The average survival is around 62 days for the SVZ EGFR wt/amp and around 32 days for the SVZ EGFR vIII cells, showing a proliferation rate of more than 10% and 30% in SVZ EGFR wt/amp and SVZ EGFR vIII tumors, respectively. Both mouse glioma models showed a complete dependence on EGFR activity, since their growth can be impaired by a tyrosin kinase inhibitor (dacomitinib) (44). NPA (NRAS, shP53, shATRX) IDH1 wt and NPA (NRAS, shP53, shATRX) IDH1 R132H were provided by Maria G. Castro (University of Michigan) (14) and cultured in CM.

Statistical analysis

For bar graphs, the significance was determined by a two-tailed un-paired Student´s t-test. The difference between experimental groups was assessed by Paired t-Test and one-way ANOVA. For Kaplan-Meier survival curves, the significance was determined by the two-tailed log-rank test. For correlation analysis between each gene, expression data were tested by Pearson's correlation coefficient and Spearman´s correlation coefficient. All analyses were performed with the GraphPad Prism 5 software. P values < 0.05 were considered significant (*p < 0.05; **p < 0.01; *** p< 0.001; **** p< 0.0001; n.s., non-significant). All quantitative data presented are the mean ± SEM from at least three simples or experiments per data point. Precise experimental details (number of animals or cells and experimental replicates) are provided in the Figure legends.
Aditional information can be found in Supplementary Materials and Methods

SUPPLEMENTARY MATERIALS

Fig. S1. Association of Tau quantity with the clinical pathology of diffuse gliomas.

Fig. S2. Patients derived Xenograft (PDXs) show a specific expression of Tau.

Supplementary Materials and Methods

References

1. Louis,D.N., Perry,A., Reifenberger,G., von,D.A., Figarella-Branger,D., Cavenee,W.K., Ohgaki,H., Wiestler,O.D., Kleihues,P., and Ellison,D.W. 2016. The 2016 World Health Organization Classification of Tumors of the Central Nervous System: a summary. *Acta Neuropathol.* **131**:803-820.

2. Yan,H., Parsons,D.W., Jin,G., McLendon,R., Rasheed,B.A., Yuan,W., Kos,I., Batinic-Haberle,I., Jones,S., Riggins,G.J. et al 2009. IDH1 and IDH2 mutations in gliomas. *N Engl J Med* **360**:765-773.

3. Turcan,S., Rohle,D., Goenka,A., Walsh,L.A., Fang,F., Yilmaz,E., Campos,C., Fabius,A.W., Lu,C., Ward,P.S. et al 2012. IDH1 mutation is sufficient to establish the glioma hypermethylator phenotype. *Nature* **483**:479-483.

4. Lu,C., Ward,P.S., Kapoor,G.S., Rohle,D., Turcan,S., Abdel-Wahab,O., Edwards,C.R., Khanin,R., Figueroa,M.E., Melnick,A. et al 2012. IDH mutation impairs histone demethylation and results in a block to cell differentiation. *Nature* **483**:474-478.

5. Calvert,A.E., Chalastanis,A., Wu,Y., Hurley,L.A., Kouri,F.M., Bi,Y., Kachman,M., May,J.L., Bartom,E., Hua,Y. et al 2017. Cancer-Associated IDH1 Promotes Growth and Resistance to Targeted Therapies in the Absence of Mutation. *Cell Rep.* **19**:1858-1873.

6. Molenaar,R.J., Maciejewski,J.P., Wilmink,J.W., and van Noorden,C.J.F. 2018. Wild-type and mutated IDH1/2 enzymes and therapy responses. *Oncogene* **37**:1949-1960.

7. Verhaak,R.G., Hoadley,K.A., Purdom,E., Wang,V., Qi,Y., Wilkerson,M.D., Miller,C.R., Ding,L., Golub,T., Mesirov,J.P. et al 2010. Integrated genomic analysis identifies clinically relevant subtypes of glioblastoma characterized by abnormalities in PDGFRA, IDH1, EGFR, and NF1. *Cancer Cell* **17**:98-110.

8. Ichimura,K., Narita,Y., and Hawkins,C.E. 2015. Diffusely infiltrating astrocytomas: pathology, molecular mechanisms and markers. *Acta Neuropathol.* **129**:789-808.

9. Avila,J., de Barreda,E.G., Fuster-Matanzo,A., Simon,D., Llorens-Martin,M., Engel,T., Lucas,J.J., Diaz-Hernandez,M., and Hernandez,F. 2012. Looking for novel functions of tau. *Biochem. Soc. Trans.* **40**:653-655.

10. Barreda,E.G., and Avila,J. 2011. Tau regulates the subcellular localization of calmodulin. *Biochem. Biophys. Res. Commun.* **408**:500-504.

11. Li,H., Duan,Z.W., Xie,P., Liu,Y.R., Wang,W.C., Dou,S.X., and Wang,P.Y. 2012. Effects of paclitaxel on EGFR endocytic trafficking revealed using quantum dot tracking in single cells. *PLoS. One.* **7**:e45465.

12. Lehrer,S. 2010. Glioblastoma and dementia may share a common cause. *Med. Hypotheses* **75**:67-68.

13. Gargini,R., Segura-Collar,B., and Sanchez-Gomez,P. 2019. Novel Functions of the Neurodegenerative-Related Gene Tau in Cancer. *Front Aging Neurosci.* **11**:231.

14. Nunez,F.J., Mendez,F.M., Kadiyala,P., Alghamri,M.S., Savelieff,M.G., Garcia-Fabiani,M.B., Haase,S., Koschmann,C., Calinescu,A.A., Kamran,N. et al 2019. IDH1-R132H acts as a tumor suppressor in glioma via epigenetic up-regulation of the DNA damage response. *Sci. Transl. Med.* **11**.

15. Flavahan,W.A., Drier,Y., Liau,B.B., Gillespie,S.M., Venteicher,A.S., Stemmer-Rachamimov,A.O., Suva,M.L., and Bernstein,B.E. 2016. Insulator dysfunction and oncogene activation in IDH mutant gliomas. *Nature* **529**:110-114.

16. Caillet-Boudin,M.L., Buee,L., Sergeant,N., and Lefebvre,B. 2015. Regulation of human MAPT gene expression. *Mol. Neurodegener.* **10**:28.

17. Perez,M., Santa-Maria,I., Gomez de,B.E., Zhu,X., Cuadros,R., Cabrero,J.R., Sanchez-Madrid,F., Dawson,H.N., Vitek,M.P., Perry,G. et al 2009. Tau--an inhibitor of deacetylase HDAC6 function. *J. Neurochem.* **109**:1756-1766.

18. Gao,Y.S., Hubbert,C.C., and Yao,T.P. 2010. The microtubule-associated histone deacetylase 6 (HDAC6) regulates epidermal growth factor receptor (EGFR) endocytic trafficking and degradation. *J. Biol. Chem.* **285**:11219-11226.

19. Zhang,B., Carroll,J., Trojanowski,J.Q., Yao,Y., Iba,M., Potuzak,J.S., Hogan,A.M., Xie,S.X., Ballatore,C., Smith,A.B., III et al 2012. The microtubule-stabilizing agent, epothilone D, reduces axonal dysfunction, neurotoxicity, cognitive deficits, and Alzheimer-like pathology in an interventional study with aged tau transgenic mice. *J. Neurosci.* **32**:3601-3611.

20. Bhat,K.P., Balasubramaniyan,V., Vaillant,B., Ezhilarasan,R., Hummelink,K., Hollingsworth,F., Wani,K., Heathcock,L., James,J.D., Goodman,L.D. et al 2013. Mesenchymal differentiation mediated by NF-kappaB promotes radiation resistance in glioblastoma. *Cancer Cell* **24**:331-346.

21. Pozo,N., Zahonero,C., Fernandez,P., Linares,J.M., Ayuso,A., Hagiwara,M., Perez,A., Ricoy,J.R., Hernandez-Lain,A., Sepulveda,J.M. et al 2013. Inhibition of DYRK1A destabilizes EGFR and reduces EGFR-dependent glioblastoma growth. *J Clin Invest* **123**:2475-2487.

22. Lu,F., Chen,Y., Zhao,C., Wang,H., He,D., Xu,L., Wang,J., He,X., Deng,Y., Lu,E.E. et al 2016. Olig2-Dependent Reciprocal Shift in PDGF and EGF Receptor Signaling Regulates Tumor Phenotype and Mitotic Growth in Malignant Glioma. *Cancer Cell* **29**:669-683.

23. Garcia-Romero,N., Gonzalez-Tejedo,C., Carrion-Navarro,J., Esteban-Rubio,S., Rackov,G., Rodriguez-Fanjul,V., Oliver-De La Cruz,J., Prat-Acin,R., Peris-Celda,M., Blesa,D. et al 2016. Cancer stem cells from human glioblastoma resemble but do not mimic original tumors after in vitro passaging in serum-free media. *Oncotarget.* **7**:65888-65901.

24. Bougnaud,S., Golebiewska,A., Oudin,A., Keunen,O., Harter,P.N., Mader,L., Azuaje,F., Fritah,S., Stieber,D., Kaoma,T. et al 2016. Molecular crosstalk between tumour and brain parenchyma instructs histopathological features in glioblastoma. *Oncotarget.* **7**:31955-31971.

25. Bergers,G., and Song,S. 2005. The role of pericytes in blood-vessel formation and maintenance. *Neuro. Oncol.* **7**:452-464.

26. Scully,S., Francescone,R., Faibish,M., Bentley,B., Taylor,S.L., Oh,D., Schapiro,R., Moral,L., Yan,W., and Shao,R. 2012. Transdifferentiation of glioblastoma stem-like cells into mural cells drives vasculogenic mimicry in glioblastomas. *J. Neurosci.* **32**:12950-12960.

27. Cheng,L., Huang,Z., Zhou,W., Wu,Q., Donnola,S., Liu,J.K., Fang,X., Sloan,A.E., Mao,Y., Lathia,J.D. et al 2013. Glioblastoma stem cells generate vascular pericytes to support vessel function and tumor growth. *Cell* **153**:139-152.

28. Zhou,W., Chen,C., Shi,Y., Wu,Q., Gimple,R.C., Fang,X., Huang,Z., Zhai,K., Ke,S.Q., Ping,Y.F. et al 2017. Targeting Glioma Stem Cell-Derived Pericytes Disrupts the Blood-Tumor Barrier and Improves Chemotherapeutic Efficacy. *Cell Stem Cell* **21**:591-603.

29. Hardee,M.E., and Zagzag,D. 2012. Mechanisms of glioma-associated neovascularization. *Am. J. Pathol.* **181**:1126-1141.

30. Park,J.S., Kim,I.K., Han,S., Park,I., Kim,C., Bae,J., Oh,S.J., Lee,S., Kim,J.H., Woo,D.C. et al 2016. Normalization of Tumor Vessels by Tie2 Activation and Ang2 Inhibition Enhances Drug Delivery and Produces a Favorable Tumor Microenvironment. *Cancer Cell* **30**:953-967.

31. Simonavicius,N., Robertson,D., Bax,D.A., Jones,C., Huijbers,I.J., and Isacke,C.M. 2008. Endosialin (CD248) is a marker of tumor-associated pericytes in high-grade glioma. *Mod. Pathol.* **21**:308-315.

32. Buckner,J.C., Chakravarti,A., and Curran,W.J., Jr. 2016. Radiation plus Chemotherapy in Low-Grade Glioma. *N. Engl. J. Med.* **375**:490-491.

33. Cairncross,J.G., Wang,M., Jenkins,R.B., Shaw,E.G., Giannini,C., Brachman,D.G., Buckner,J.C., Fink,K.L., Souhami,L., Laperriere,N.J. et al 2014. Benefit from procarbazine, lomustine, and vincristine in oligodendroglial tumors is associated with mutation of IDH. *J. Clin. Oncol.* **32**:783-790.

34. Amankulor,N.M., Kim,Y., Arora,S., Kargl,J., Szulzewsky,F., Hanke,M., Margineantu,D.H., Rao,A., Bolouri,H., Delrow,J. et al 2017. Mutant IDH1 regulates the tumor-associated immune system in gliomas. *Genes Dev.* **31**:774-786.

35. Yao,Y., Chan,A.K., Qin,Z.Y., Chen,L.C., Zhang,X., Pang,J.C., Li,H.M., Wang,Y., Mao,Y., Ng,H.K. et al 2013. Mutation analysis of IDH1 in paired gliomas revealed IDH1 mutation was not associated with malignant progression but predicted longer survival. *PLoS. One.* **8**:e67421.

36. Johnson,B.E., Mazor,T., Hong,C., Barnes,M., Aihara,K., McLean,C.Y., Fouse,S.D., Yamamoto,S., Ueda,H., Tatsuno,K. et al 2014. Mutational analysis reveals the origin and therapy-driven evolution of recurrent glioma. *Science* **343**:189-193.

37. Watanabe,T., Nobusawa,S., Kleihues,P., and Ohgaki,H. 2009. IDH1 mutations are early events in the development of astrocytomas and oligodendrogliomas. *Am. J. Pathol.* **174**:1149-1153.

38. Bardella,C., Al-Dalahmah,O., Krell,D., Brazauskas,P., Al-Qahtani,K., Tomkova,M., Adam,J., Serres,S., Lockstone,H., Freeman-Mills,L. et al 2016. Expression of Idh1(R132H) in the Murine Subventricular Zone Stem Cell Niche Recapitulates Features of Early Gliomagenesis. *Cancer Cell* **30**:578-594.

39. Philip,B., Yu,D.X., Silvis,M.R., Shin,C.H., Robinson,J.P., Robinson,G.L., Welker,A.E., Angel,S.N., Tripp,S.R., Sonnen,J.A. et al 2018. Mutant IDH1 Promotes Glioma Formation In Vivo. *Cell Rep.* **23**:1553-1564.

40. Rohle,D., Popovici-Muller,J., Palaskas,N., Turcan,S., Grommes,C., Campos,C., Tsoi,J., Clark,O., Oldrini,B., Komisopoulou,E. et al 2013. An inhibitor of mutant IDH1 delays growth and promotes differentiation of glioma cells. *Science* **340**:626-630.

41. Golub,D., Iyengar,N., Dogra,S., Wong,T., Bready,D., Tang,K., Modrek,A.S., and Placantonakis,D.G. 2019. Mutant Isocitrate Dehydrogenase Inhibitors as Targeted Cancer Therapeutics. *Front Oncol.* **9**:417.

42. Molenaar,R.J., Botman,D., Smits,M.A., Hira,V.V., van Lith,S.A., Stap,J., Henneman,P., Khurshed,M., Lenting,K., Mul,A.N. et al 2015. Radioprotection of IDH1-Mutated Cancer Cells by the IDH1-Mutant Inhibitor AGI-5198. *Cancer Res.* **75**:4790-4802.

43. Khurshed,M., Aarnoudse,N., Hulsbos,R., Hira,V.V.V., van Laarhoven,H.W.M., Wilmink,J.W., Molenaar,R.J., and van Noorden,C.J.F. 2018. IDH1-mutant cancer cells are sensitive to cisplatin and an IDH1-mutant inhibitor counteracts this sensitivity. *FASEB J.*fj201800547R.

44. Wu,X., Sooman,L., Lennartsson,J., Bergstrom,S., Bergqvist,M., Gullbo,J., and Ekman,S. 2013. Microtubule inhibition causes epidermal growth factor receptor inactivation in oesophageal cancer cells. *Int. J. Oncol.* **42**:297-304.

45. Zahonero,C., and Sanchez-Gomez,P. 2014. EGFR-dependent mechanisms in glioblastoma: towards a better therapeutic strategy. *Cell Mol. Life Sci*.

46. Grandal,M.V., Zandi,R., Pedersen,M.W., Willumsen,B.M., van,D.B., and Poulsen,H.S. 2007. EGFRvIII escapes down-regulation due to impaired internalization and sorting to lysosomes. *Carcinogenesis* **28**:1408-1417.

47. Bonavia,R., Inda,M.M., Vandenberg,S., Cheng,S.Y., Nagane,M., Hadwiger,P., Tan,P., Sah,D.W., Cavenee,W.K., and Furnari,F.B. 2012. EGFRvIII promotes glioma angiogenesis and growth through the NF-kappaB, interleukin-8 pathway. *Oncogene* **31**:4054-4066.

48. Gargini,R., Escoll,M., Garcia,E., Garcia-Escudero,R., Wandosell,F., and Anton,I.M. 2016. WIP Drives Tumor Progression through YAP/TAZ-Dependent Autonomous Cell Growth. *Cell Rep.* **17**:1962-1977.

49. Ferraiuolo,M., Pulito,C., Finch-Edmondson,M., Korita,E., Maidecchi,A., Donzelli,S., Muti,P., Serra,M., Sudol,M., Strano,S. et al 2018. Agave negatively regulates YAP and TAZ transcriptionally and post-translationally in osteosarcoma cell lines. *Cancer Lett.* **433**:18-32.

50. Lai,A., Kharbanda,S., Pope,W.B., Tran,A., Solis,O.E., Peale,F., Forrest,W.F., Pujara,K., Carrillo,J.A., Pandita,A. et al 2011. Evidence for sequenced molecular evolution of IDH1 mutant glioblastoma from a distinct cell of origin. *J. Clin. Oncol.* **29**:4482-4490.

51. Unruh,D., Schwarze,S.R., Khoury,L., Thomas,C., Wu,M., Chen,L., Chen,R., Liu,Y., Schwartz,M.A., Amidei,C. et al 2016. Mutant IDH1 and thrombosis in gliomas. *Acta Neuropathol.* **132**:917-930.

52. Kickingereder,P., Sahm,F., Radbruch,A., Wick,W., Heiland,S., Deimling,A., Bendszus,M., and Wiestler,B. 2015. IDH mutation status is associated with a distinct hypoxia/angiogenesis transcriptome signature which is non-invasively predictable with rCBV imaging in human glioma. *Sci. Rep.* **5**:16238.

53. Missiaen,R., Mazzone,M., and Bergers,G. 2018. The reciprocal function and regulation of tumor vessels and immune cells offers new therapeutic opportunities in cancer. *Semin. Cancer Biol.* **52**:107-116.

54. Pallas-Bazarra,N., Jurado-Arjona,J., Navarrete,M., Esteban,J.A., Hernandez,F., Avila,J., and Llorens-Martin,M. 2016. Novel function of Tau in regulating the effects of external stimuli on adult hippocampal neurogenesis. *EMBO J.* **35**:1417-1436.

55. Podtelezhnikov,A.A., Tanis,K.Q., Nebozhyn,M., Ray,W.J., Stone,D.J., and Loboda,A.P. 2011. Molecular insights into the pathogenesis of Alzheimer's disease and its relationship to normal aging. *PLoS. One.* **6**:e29610.

56. Kisler,K., Nelson,A.R., Montagne,A., and Zlokovic,B.V. 2017. Cerebral blood flow regulation and neurovascular dysfunction in Alzheimer disease. *Nat. Rev. Neurosci.* **18**:419-434.

57. Sagare,A.P., Bell,R.D., Zhao,Z., Ma,Q., Winkler,E.A., Ramanathan,A., and Zlokovic,B.V. 2013. Pericyte loss influences Alzheimer-like neurodegeneration in mice. *Nat. Commun.* **4**:2932.

58. Semiond,D., Sidhu,S.S., Bissery,M.C., and Vrignaud,P. 2013. Can taxanes provide benefit in patients with CNS tumors and in pediatric patients with tumors? An update on the preclinical development of cabazitaxel. *Cancer Chemother. Pharmacol.* **72**:515-528.

59. Smoter,M., Bodnar,L., Duchnowska,R., Stec,R., Grala,B., and Szczylik,C. 2011. The role of Tau protein in resistance to paclitaxel. *Cancer Chemother. Pharmacol.* **68**:553-557.

60. Ferron,S.R., Andreu-Agullo,C., Mira,H., Sanchez,P., Marques-Torrejon,M.A., and Farinas,I. 2007. A combined ex/in vivo assay to detect effects of exogenously added factors in neural stem cells. *Nat. Protoc.* **2**:849-859.

Figure captions

Fig. 1. Tau is expressed in gliomas and it is enriched in LGG. (**A**) Analysis of *Tau (MAPT)* mRNA expression by RNAseq in gliomas (TCGA cohort) grouped according to the WHO classification (n=692). (**B** and **C**) Kaplan-Meier overall survival curves of patients from the TCGA (LGG+GBM) (n=664) and the Rembrandt (LGG+GBM) (n=396) cohorts. Patients in each cohort were stratified into 2 groups based on high and low *Tau (MAPT)* expression values; log-rank (Mantel-Cox) test. (**D**) Representative pictures of the Tau IHC staining in gliomas and normal tissue (NT). The Tau IHC score is represented between brackets and an amplified section of the last three images is shown on the bottom. (**E**) WB analysis of Tau in tumor tissue extracts from patients diagnosed with LGG (red) and GBM (blue). NT was used as a control of Tau expression and GAPDH as a loading control. (**F**) Percentage of tumors (GBM (n=55) and LGG (n=22)) with different Tau IHC score. (**G**) Quantification of the relative amount of Tau in the WB in E. Data shown as mean ± SD; Student's t test; ****, $p \leq 0.0001$. n.s. non significant. Scale bar 50 μm.

Fig. 2. Tau correlates inversely with glioma aggressiveness. (**A** to **C**) Kaplan-Meier overall survival curves of patients from the TCGA GBM cohort (n=264) (A), the TCGA LGG cohort (n= 155) and our own GBM cohort (n=30) (C). Patients in each cohort were stratified into 2 groups based on high and low *Tau (MAPT)* expression values (RNAseq in A and B, and qRT-PCR in C (*HPRT* was used for normalization)); log-rank (Mantel-Cox) test. (**D**) Analysis of *Tau (MAPT)* mRNA expression by RNAseq in gliomas (TCGA cohort) grouped according to the clinical evolution of the tumors (n=386). (**E** and **F**) Representative pictures of the Tau IHC staining of paired glioma samples (primary and recurrent tumor). Average Tau IHC score of the paired samples in shown on the right. (**G**) WB analysis of Tau expression in tumor tissue extracts from subcutaneous PDXs. The same extract from 12o53F cells was loaded in both gels for comparison.GAPDH was used as a loading control. (**H**) Kaplan-Meier overall survival curves of mice that were orthotopically injected with different primary GBM cell lines; log-rank (Mantel-Cox) test. (**I**) qRT-PCR analysis of *Tau (MAPT)* expression in tumor tissue extracts from (H). *HPRT* was used for normalization. (**J**) Kaplan-Meier overall survival curves of mice that were orthotopically injected with 12o15 cells overexpressing GFP or Tau (n=6). (**K**) Kaplan-Meier overall survival curves of mice that were orthotopically injected with 12o02 control or 12o02-shTau cells (n=6); log-rank (Mantel-Cox) test. Data shown as mean ± SD; Student's t test; **, $p \leq 0.01$; ****, $p \leq 0.0001$. Scale bar 50 μm.

Fig. 3. *Tau* expression is regulated by IDH1/2 function. (**A**) Analysis of non-silent somatic mutations in genes commonly modified in diffuse glioma grouped based on high or low expression of *Tau (MAPT)*. (**B**) Volcano plots showing mutated genes with differential distribution in glioma comparing tumors with high and low *Tau*. The arrow points to *IDH1* mutations. (**C**) Percentage of tumors with different Tau IHC score in wt (n= 35) and mutant (n=36) *IDH1* gliomas. (**D**) Kaplan-Meier overall survival curves of mice that were orthotopically injected with NPA IDH1 wt or NPA-IDH1 R132H cells (n=6); log-rank (Mantel-Cox) test. (**E**) WB analysis and quantification of Tau expression in intracranial tumors from (D). Actin was used as loading control. (**F**) Quantification of the methylation of CpG26 using 5 different probes and comparing IDHwt vs IDHmut gliomas. (**G**) CTCF-binding profiles for the *Tau (MAPT*) CpG26 locus in IDH-mutant and IDH wild-type tumors, normalized by average signal. (**H**) Analysis of the expression of Tau (*MAPT)* gene expression by qPCR in the presence of increasing amounts of 2-hydroxy-glutarate (2-HG) in RG1, 12o15, GB4 and GB18 cells. (**I**) Analysis of the expression of Tau (*MAPT)* gene expression by qRT-PCR in RG1 cells cultured in the presence of 1 mM of the 2-HG, with or without azacytidine (AZA) (1 μM)(n=3). (**J** and **K**) Correlation of the expression of *Tau (MAPT)* with that of wild-type *IDH1* using the TCGA-merge (LGG+GBM) (n=669) (J) and the Rembrandt (LGG+GBM) (n=580) (K) cohorts, Pearson's correlation test. Data shown as mean ± SD; Student's t test; *, $p \leq 0.05$; **, $p \leq 0.01$; ****, #, $p \leq 1x10^{-90}$.

Fig. 4. Tau opposes EGFR in gliomas. (**A**) Distribution of somatic non-silent mutations in *IDH1/2*, *EGFR* and *PTEN* in a glioma cohort (TCGA, n=812). (**B**) Volcano plots showing mutated genes with differential distribution in gliomas, comparing tumors with high and low *Tau*. The arrows point to *PTEN* and *EGFR* mutations. (**C**) Kaplan-Meier overall survival curves of mice that were orthotopically injected with RG1, RG1 IDH1 wt or RG1 IDH1 R32H cells (n=6); log-rank (Mantel-Cox) test. (**D**) WB analysis of phosphorylated EGFR (pEGFR) and Tau in intracranial tumors from (C). Actin was used as a loading control. (**E**) Quantification of the amount of Tau in (D). (**F**) Correlation between Tau and phospho-EGFR in RG1 tumors, Pearson's correlation test.. (**G** and **H**) Kaplan-Meier overall survival curves of patients from the LGG+GBM TCGA cohort. Patients were separated based on the *EGFR* status: tumors without mutations (amplified or wild type) (n=114) (G) and amplified tumors with mutations (n=54) (H). Then, they were stratified into 2 groups based on *Tau (MAPT)* expression value; log-rank (Mantel-Cox) test. (**I** to **L)** Kaplan-Meier overall survival curves of mice that were orthotopically injected with SVZ-EGFRamp/wt (I), SVZ-EGFRvIII (J), RG1 (*EGFR*amp) (K) or 12o150

(*EGFR*mut) (L) cells, overexpressing either GFP or Tau (n=6); log-rank (Mantel-Cox) test. Data shown as mean ± SD; Student's t test; **, $p \leq 0.01$.

Fig. 5. Tau and microtubule-stabilizing compounds impair EGFRwt stability and signaling in gliomas. (**A** to **D**) WB analysis and quantification of phosphorylated EGFR (pEGFR) in SVZ EGFRwt/amp (A), RG1 (B), SVZ EGFR vIII (C) and 12o150 (D) tumors after the overexpression of GFP or Tau. Actin was used as a loading control. (**E**) WB analysis of total EGFR and Acetylated tubulin (Acetyl-tub) in SVZ EGFR wt/amp and RG1 tumors after the overexpression of GFP or Tau. Actin was used as a loading control. (**F**) WB analysis of total EGFR in SVZ EGFRwt/amp and SVZ EGFR vIII cells after the overexpression of GFP or Tau, in the absence or in the presence of MG123 (MG, 10 μM) and Chloroquine (CLQ, 200 μM). (**G**) Kaplan-Meier overall survival curves of mice that were orthotopically injected with RG1 cells and subsequently treated with intraperitoneal injections (2/week) of EpoD (1 mg/Kg) (n=8); log-rank (Mantel-Cox) test. (**H** and **I**) WB analysis and quantification of pEGFR, total EGFR and Acetyl-tub in the tumors (G). Actin was used as loading control. (**J**) Kaplan-Meier overall survival curves of mice that were orthotopically injected with RG1 cells and subsequently treated with intraperitoneal injections (2/week) of EpoD (1mg/Kg) and/or TMZ (5mg/Kg/day) (n=6); log-rank (Mantel-Cox) test. Data shown as mean ± SD; Student's t test; *, $p \leq 0.05$, **, $p \leq 0.01$, ***, $p \leq 0.001$; n.s. non significant.

Fig. 6. Tau blocks the mesenchymal features of *EGFR*amp/wt cells through the inhibition of the EGFR/NF-κB/TAZ axis. (**A**) Heatmap of PN, MES, neuronal differentiation, PDGFRα pathway, NF-κB/inflammation, and hypoxia-related cancer expression genes depending on *Tau (MAPT)* expression. (**B**) GSEA enrichment plot analysis using Tau gene expression values as template and the NF-κB pathway geneset from the Biocarta pathways database. (**C** to **F**) WB analysis (**C** and **E**) and quantification (**D** and **F**) of phosphorylated EGFR (pEGFR), phosphorylated pNF-κB (p65) and TAZ in RG1 (**C** and **D**) and 12o15 (**E** and **F**) xenografts expressing either GFP or Tau. GADPH was used as a loading control (n=3). (**G** and **H**) qRT-PCR analysis of MES (G) and PN-subtype (H) related genes in RG1 xenografts expressing GFP or Tau. *HPRT* was used for normalization. (**I**) Representative images of TAZ (top) or OLIG2 (bottom) IF staining of sections from GFP or Tau overexpressing RG1 gliomas. Quantification is shown on the right. **(J** and **K**) qRT-PCR analysis of *TAZ* (J) and *OLIG2* (K) in gliomas (n=6). Tumors were classified in two groups based on the expression of *Tau (MAPT)*. (n=72). *HPRT* expression was used for normalization. (**L**) Kaplan-Meier overall survival curves of mice

that were orthotopically injected with RG1 cells overexpressing GFP, Tau or GFP, Tau plus TAZ (n=6); log-rank (Mantel-Cox) test. (**M**) WB analysis of TAZ in the tumors (L). Actin was using as loading control. (**N**) Kaplan-Meier overall survival curves of mice that were orthotopically injected with RG1 shControl or RG1 shTAZ cells (n=6); log-rank (Mantel-Cox) test. (**O**) qRT-PCR analysis of pericytic–related genes in the tumors (N). (**P** to **R**) WB analysis (**P**) and quantification (**Q** and **R**) of TAZ, αSMA, NG2 and CD248 in RG1 (P and Q) or 12O15 (P and R) cells after TAZ downregulation. GADPH was used for normalization. Data shown as mean ± SD; Student's t test; *, $p \leq 0.05$; **, $p \leq 0.01$; ***, $p \leq 0.001$; n.s. non significant. Scale bar 25 μm.

Fig. 7. Tau overexpression blocks the appearance of tumor-derived-pericytes in *EGFRwt*/amp gliomas, inhibiting angiogenesis and normalizing the tumor vasculature. (**A**) Representative images of endomucin and αSMA (top) or endomucin and CD248 (bottom) IF co-staining of sections from RG1 xenografts expressing GFP or Tau. (**B**) qRTPCR analysis of pericytic–related genes (using human-specific primers) in RG1 GFP and Tau xenografts. *HPRT* was used for normalization. (**C**) qRT-PCR analysis of pericytic–related genes (using mouse-specific primers) in RG1 GFP and Tau xenografts. *Actin* was used for normalization (n=3 to 5). (**D**) Representative images of endomucin IF staining of sections from RG1 xenografts expressing GFP or Tau. (**E**) Quantification of dilated blood vessels in (D) (indicated by arrows) (n=10). (**F**) Representative contrast phase images of HMBEC cells cultured in the presence of conditioned media from RG1 GFP or RG1 Tau cells. The number of sprouts is shown on the right. (**G**) WB of VEGF in the supernatant of RG1 cells after overexpression of GFP or Tau. LAMP2 and TUBULIN were used as loading controls. (**H**) Representative images of sectioned mouse brains (top) and pseudo-color images of Fluc bioluminescence (bottom), after the injection of GFP or Tau-expressing RG1 cells. (**I** and **J**) Representative images of IF co-staining of endomucin and IgG (I) or endomucin and Ang2 (J) on RG1 xenografts expressing GFP or Tau. (**K**) Ratio of *Ang2/Ang1* expression measured by qRT-PCR in RG1 gliomas after Tau overexpression (n=3). *Actin* was used for normalization. (**L**) Kaplan-Meier overall survival curves of mice that were orthotopically injected with RG1 cells expressing shcontrol, shCD248 55 or shCD248 21 (n=6); log-rank (Mantel-Cox) test. (**M**) qRT-PCR analysis of pericytic-related genes in RG1 tumors expressing shcontrol or shCD248 21 (n=3 to 4). (**N**) Representative images of IF co-staining of endomucin and IgG from tumors in (L). (**O**) Ratio of *Ang2/Ang1* expression measured by qRT-PCR in RG1 gliomas after *CD248* downregulation (n=3). *Actin* was used for normalization. Data shown as mean ± SD;

Student's t test; *, $p \leq 0.05$; **, $p \leq 0.01$; ***, $p \leq 0.001$; ****, $p \leq 0.0001$; n.s., nonsignificant. Scale bar 25 μm.

Fig. 8. Analysis of Tau and vascular molecules in human samples. (**A** to **E**) *Tau (MAPT)* (A and B), pEGFR (C), and CD248 (D and E) expression was determined by qRT-PCR analysis (Glioma cohort) (n=87) (A and B), RNAseq analysis (TCGA-LGG+GBM cohort) (n=319) (B and E) or by WB (n=50) (C). Tumors were classified in three groups: IDH1 wt (Tau Low), IDH1 wt (Tau High) and IDH1 mut. *HPRT* expression was used for normalization. (**F**) Representative pictures of the IHC staining of Tau, CD34 and CD48 in three tumors, one for each of the groups. (**G**) Percentage of tumors with different CD248 IHC score in F (n=68). (**H**) *CD34* transcription was determined by qRT-PCR analysis (GBM cohort) (n=87). (**I**) Quantification of the dilated blood vessels in F (n=68). Data shown as mean ± SD; Student's t test; *, $p \leq 0.05$; **, $p \leq 0.01$; ***, $p \leq 0.001$; ****, $p \leq 0.0001$. n.s., non-significant. Scale bar 100 μm.

Acknowledgments

The authors acknowledge Rosella Galli for donating RG1, Rafael Hortigüela and the Confocal service personell, for their technical support. The graphical abstract was created with images adapted from Servier Medical Art by Servier.

Funding

Work was supported by NIH/NINDS grant R01-NS105556 to MGC; by Ministerio de Economía y Competitividad: (Acción Estratégica en Salud) grants: PI13/01258 to AHL, PI17/01489 and CP11/00147 to AAS, PI18/00263 to RGE, and PI16/01 278 to JS; by "Asociación Española contra el Cancer" (AECC) grants: Investigador Junior to RG and GCTRA16015SEDA to JMS and JS; and by Ministerio de Economía y Competitividad: SAF-2014-53040-P to JA, RTC-2015-3771-1 to JS and SAF2015-65175-R/FEDER to PSG.

Author Contributions

Conceptualization: RG, BSC, JA and PSG; Investigation: RG, BSC, ARB, BH, FJN, DGP, JGG and RGE; Formal Analysis: RG and RGE; Resources: VGE, JMS, AHL, AAS, JS and MGC; Writing-Original Draft: RG, BSC, JA and PSG; Writing-Review & Editing: VGE, AAS, JS, JMS, AHL, MGC and RGE; Funding Acquisition: RG, JA and PSG; Supervision: JA and PSG.

Competing interests

JS is co-founder of Mosaic Biomedicals and Board member of Northern Biologics. JMS is a consultant for GW pharma. JS received grant/research support from Mosaic Biomedicals, Northern Biologics and Roche/Glycart; JMS received from Pfizer and PSG from from Servier, Catalysis and IDP-Pharma. The rest of the authors declare no competing financial interests.

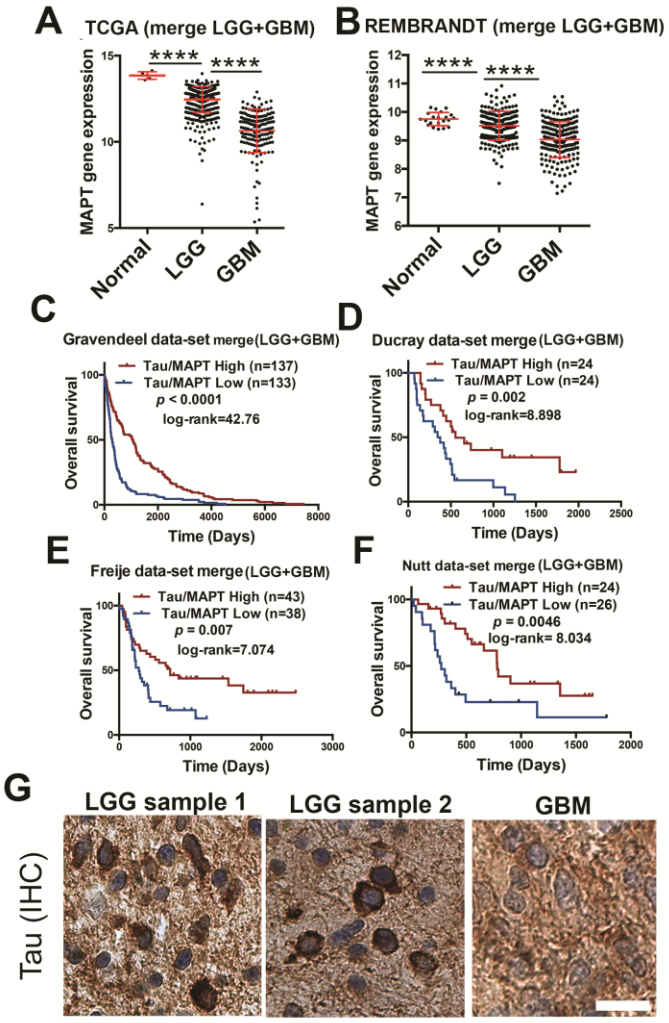

Fig. S1. Association of Tau levels with the clinical pathology of diffuse gliomas. (**A** and **B**) Analysis of *Tau (MAPT)* mRNA expression by RNAseq in diffuse glioma patients compared to normal tissue, using the TCGA (n=692) (A) and the Rembrandt (n=432) (B) cohorts. Tumors were grouped according to the WHO classification (histological type). (**C-F**) Kaplan-Meier overall survival curves of patients from the Gravendeel (n=276) (**C**); the Ducray (n=48) (**D**); the Freije (n=81) (**E**) and the Nutt (n=60) (**F**) cohorts. Patients in each cohort were stratified into 2 groups based on high and low *Tau (MAPT)* expression values, log-rank (Mantel-Cox) test. (**G**) Representative pictures of the IHC Tau staining of several gliomas. Data shown as mean ± SD; Student's t test; ****, $p \leq 0.0001$. Scale bar 20 μm.

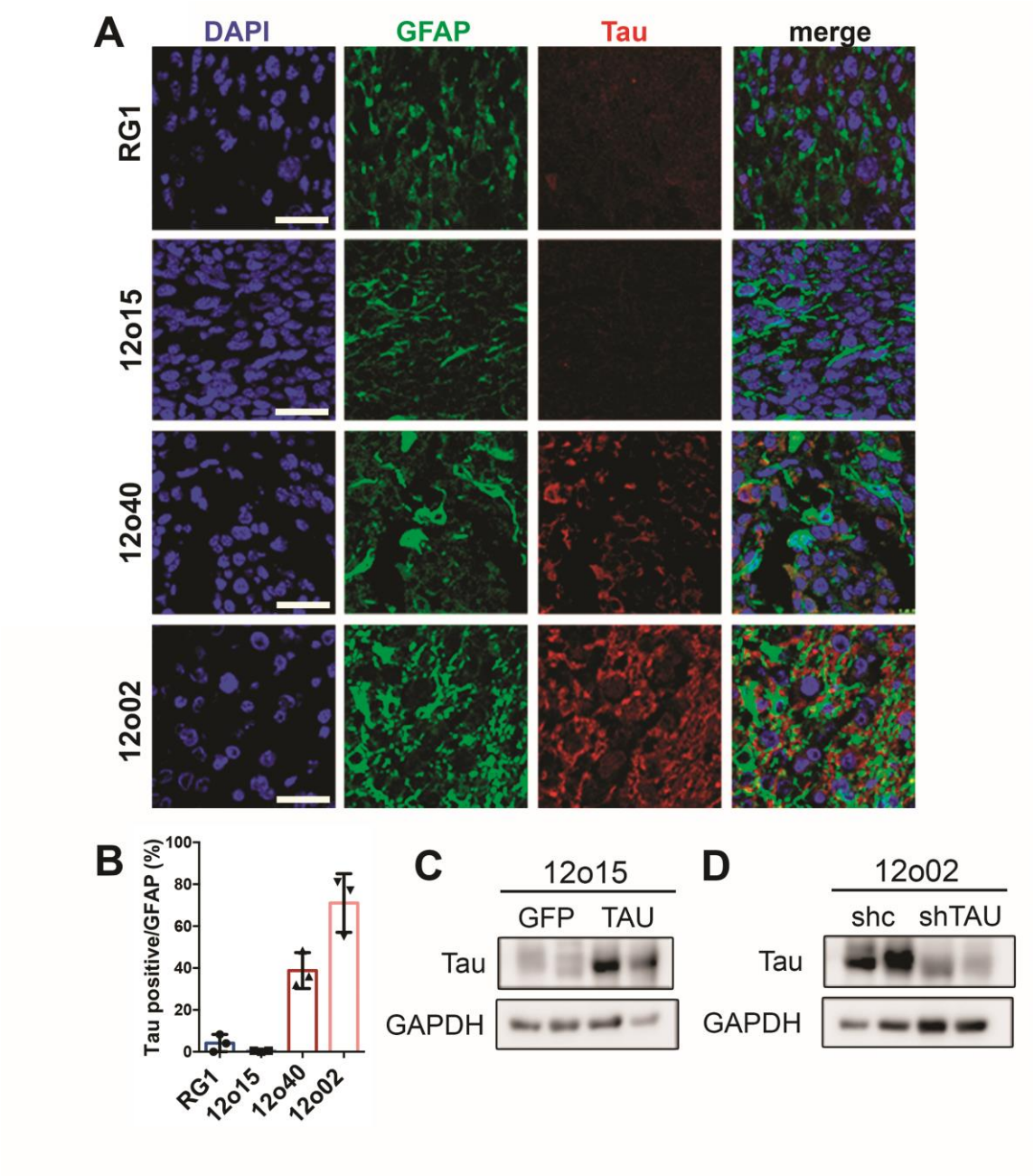

Fig. S2. (**A**) Representative images of Tau and GFAP by IF co-staining of tumors from Fig. 2H. (**B**) Quantification of the co-staining of Tau and GFAP in A. (**C-D**) WB analysis and quantification of Tau in the tumors from Fig. 2J (C) and Fig. 2K (D). GAPDH levels were used for normalization. Data shown as mean ± SD. Scale bar 50 μm.

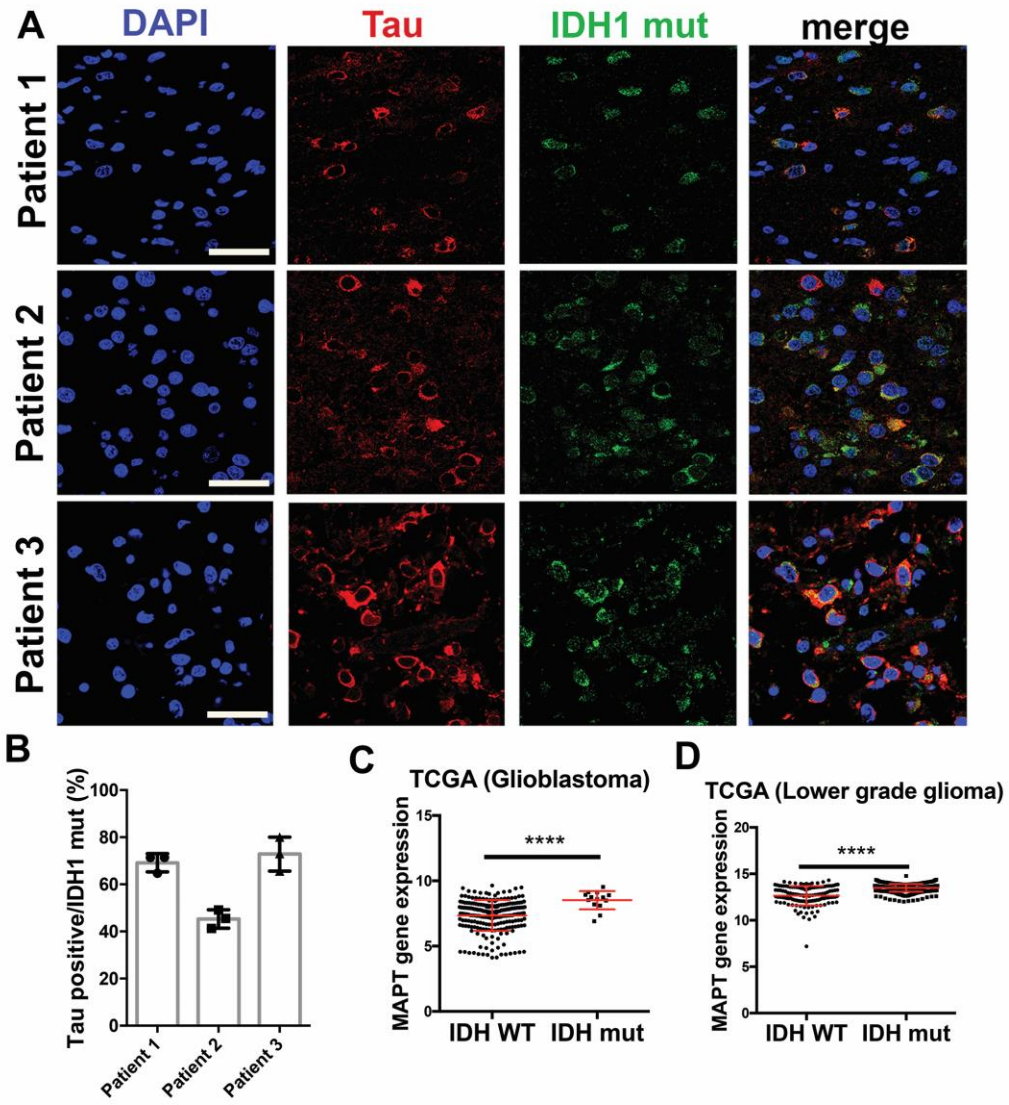

Fig. S3. Tau expression correlates with the presence of IDH mutations. (**A**) Representative images of Tau and IDH1mut IF co-staining of tumors from three different patients. (**B**) Quantification of the co-staining of Tau and IDH1mut in A (n=3). (**C** and **D**) Analysis of *Tau (MAPT)* mRNA expression by RNAseq in the GBM (C) and the LGG (D) TCGA cohorts, grouped based on the presence of IDH mutations (n=692). Data shown as mean ± SD; Student's t test; ****, $p \leq 0.0001$. Scale bar 50 μm.

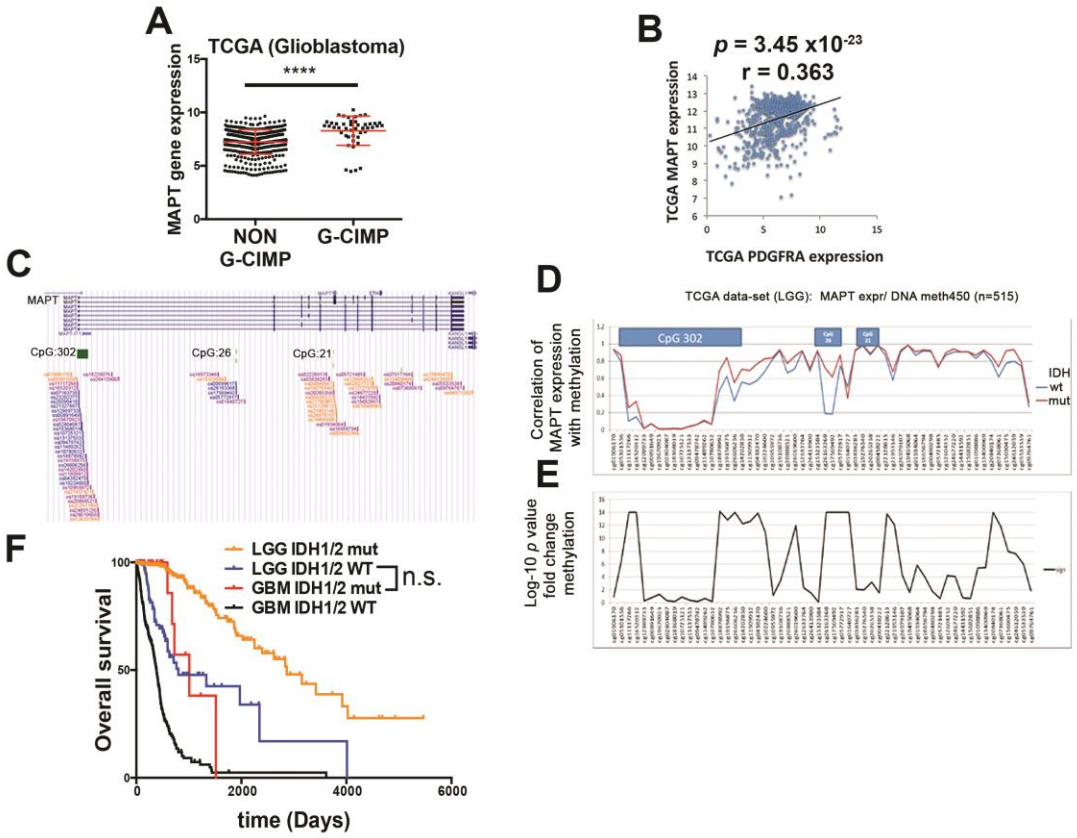

Fig. S4. The expression of Tau is associated with the IDH mutant methylation phenotype. (**A**) Analysis of *Tau (MAPT)* mRNA expression in GBM according to the level of CpG methylation: low-level methylator phenotype (NON G-CIMP) or high-level methylator phenotype (G-CIMP). (**B**) Correlation of the expression of *Tau (MAPT)* with that of *PDGFRA* (n=702) using the TCGA-merge (LGG+GBM) dataset, Pearson's correlation test. (**C**) Organization of the possible CpG islets on the promoter zone of the *Tau* (MAPT) gene using the methylation probes by genome browser. (**D** and **E**) Analysis of the fold change CpG methylation in 515 patients with LGG. The blue line shows the levels of methylation in gliomas with wildtype *IDH* and in red the level of methylation in gliomas with mutations in *IDH*. (**F**) Kaplan-Meier overall survival curves of LGG (n=451) and GBM (n=299) patients from the TCGA cohort, stratified based on the status of IDH1/2. Data shown as mean ± SD; Student's t test; ****, $p \leq 0.0001$; n.s. non significant.

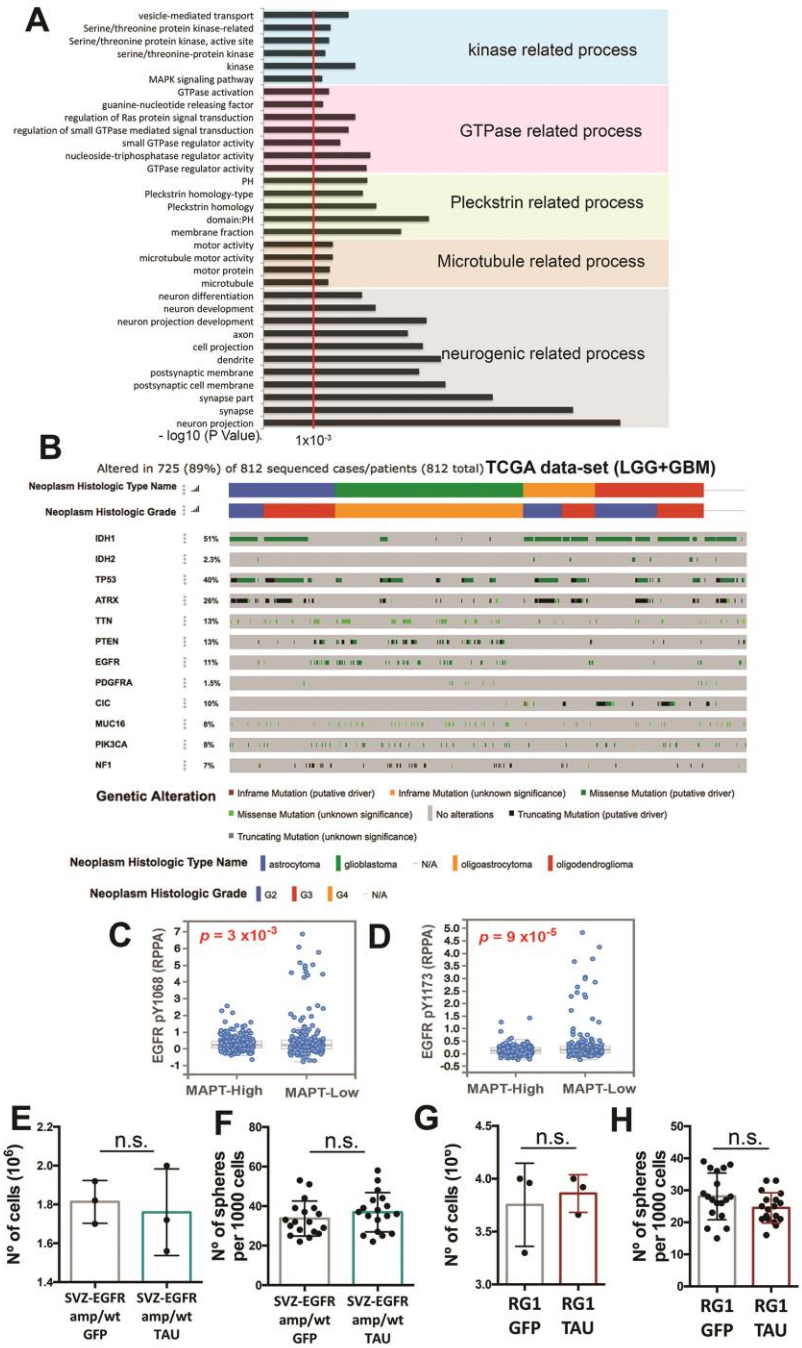

Fig. S5. Association of Tau function with the EGFR pathway in gliomas. (**A**) Top enriched Gene Ontology (GO) biological process for the cluster of 500 genes that are positively co-expressed with Tau (MAPT) in gliomas. We used the LGG+GBM merge cohort and the DAVID gene ontology program. (**B**) Histogram showing the non-silent somatic mutations in genes commonly modified in diffuse gliomas grouped according to the WHO classification (histological type and grade). (**C**) Analysis of levels of Phospho-Tyr1068-EGFR and Phospho-Tyr1173-EGFR in a cohort of 244 patients with GBM (TCGA-GBM dataset) according to high or low levels of Tau (MAPT). (**E** to **H**) Quantification of the number of cells (**E** and **G**) and spheres (**F** and **H**) in SVZ-EGFRamp/wt (**E** and **F**) and RG (**G** and **H**) cells after the overexpression of GFP or Tau (n=3). Data shown as mean ± SD; Student's t test; n.s., non-significant.

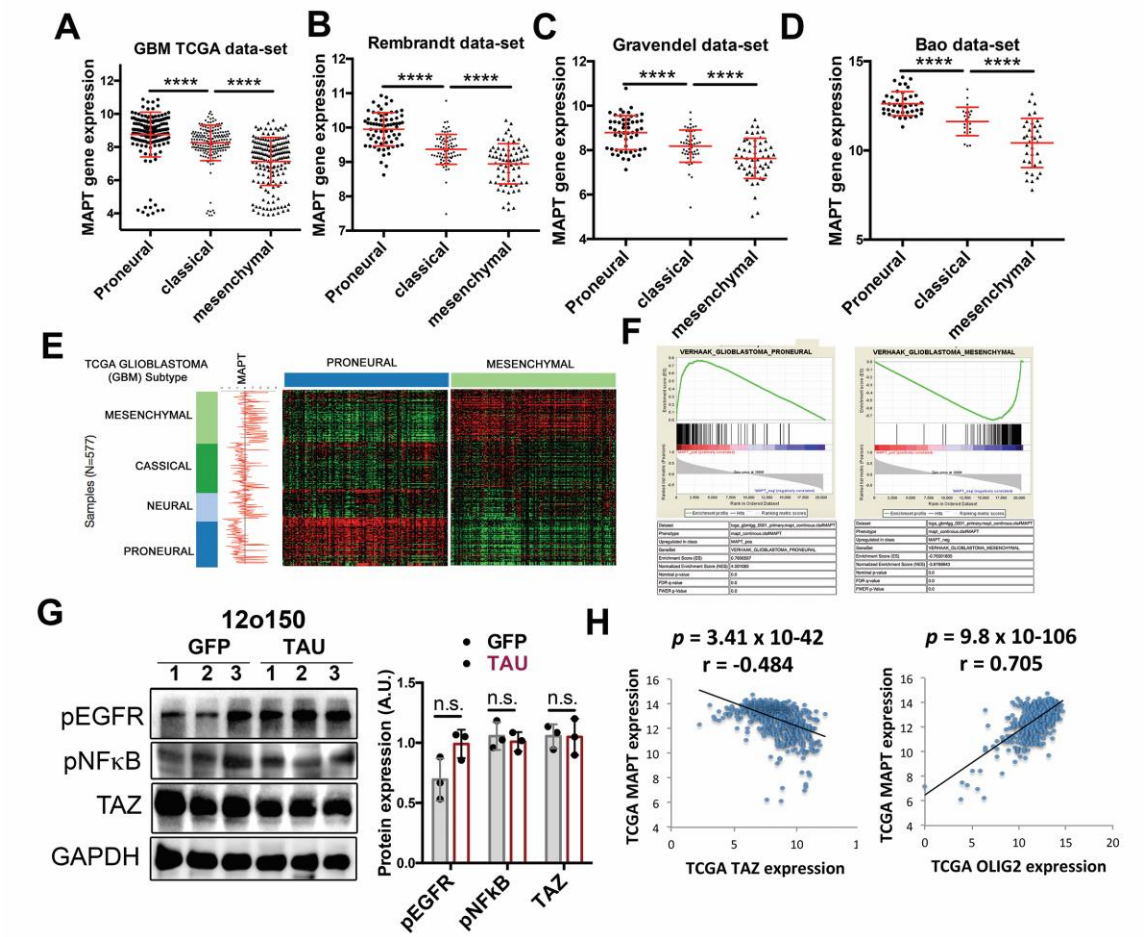

Fig. S6. Association of Tau expression with the GBM subtypes and the NF-kB-TAZ axis. (**A** to **D**) Analysis of *Tau (MAPT)* mRNA expression in the different GBM subtypes using the TCGA (n=528) (A), the Rembrandt (n=219) (B), the Gravendeel (n=159) (C) and the Bao (n=100) (D) data sets. (**E**) Heatmap of PN and MES gene expression signature depending on the levels of expression of Tau and analysis of mRNA Tau levels according to GBM subtypes. (**F**) GSEA enrichment plot analysis using Tau gene expression values as template and PN or MES signatures. (**G**) WB analysis of phospho-EGFR, phosphor-NF-κB and TAZ in 12o150 xenografts expressing either GFP or Tau. GADPH levels were used for normalization (n=3). Quantification is shown on the right. (**H**) Scatter plots showing the correlation between the expression of Tau (MAPT) and TAZ genes (left) or Tau (MAPT) and OLIG2 genes (right) across 703 glioma samples, Pearson's correlation test. Data shown as mean ± SD; Student's t test; ****, $p \leq 0.0001$; n.s., non-significant.

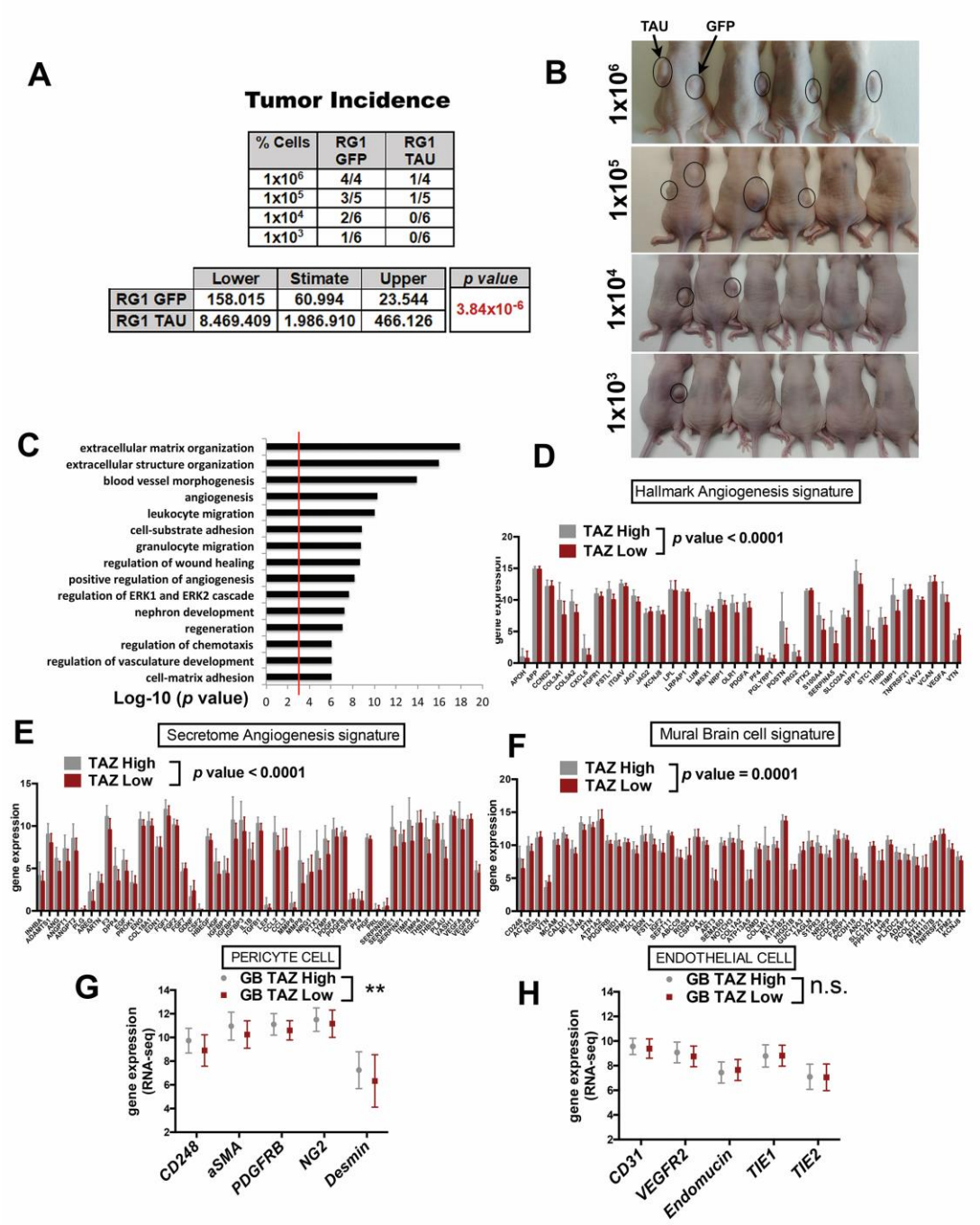

Fig. S7. Vascular phenotypes associated with TAZ in gliomas. (**A** and **B**) Subcutaneous tumor growth assay (limited dilution) of RG1 cells after overexpression of GFP or Tau (n=4 to 6). The statistical analysis is shown on the bottom and the image of the animals before tumor dissection is shown in B. (**C**) The top 15 gene ontology (GO) terms associated with cluster from the 500 genes that correlate positively with the expression of TAZ in TCGA-LGG+GBM dataset. GO terms were ranked by p value. (**D** to **F**) Angiogenesis (**D**), angiogenic secretome (**E**) and mural brain cell (**F**) signatures in gliomas of the TCGA-LGG+GBM-merge data-set. Tumors were classified as High or Low Taz-expressing gliomas (n=702). (**G** and **H**) Analysis of the expression (RNAseq) of the 5 most significant genes associated with pericytes (G) or endothelial cells (H); signature including the most relevant genes for biological processes associated with vasculogenesis, angiogenesis and secretion in (C-F). Data shown as mean ± SD; Paired t test; ** $p \leq 0.01$, n.s. non significant.

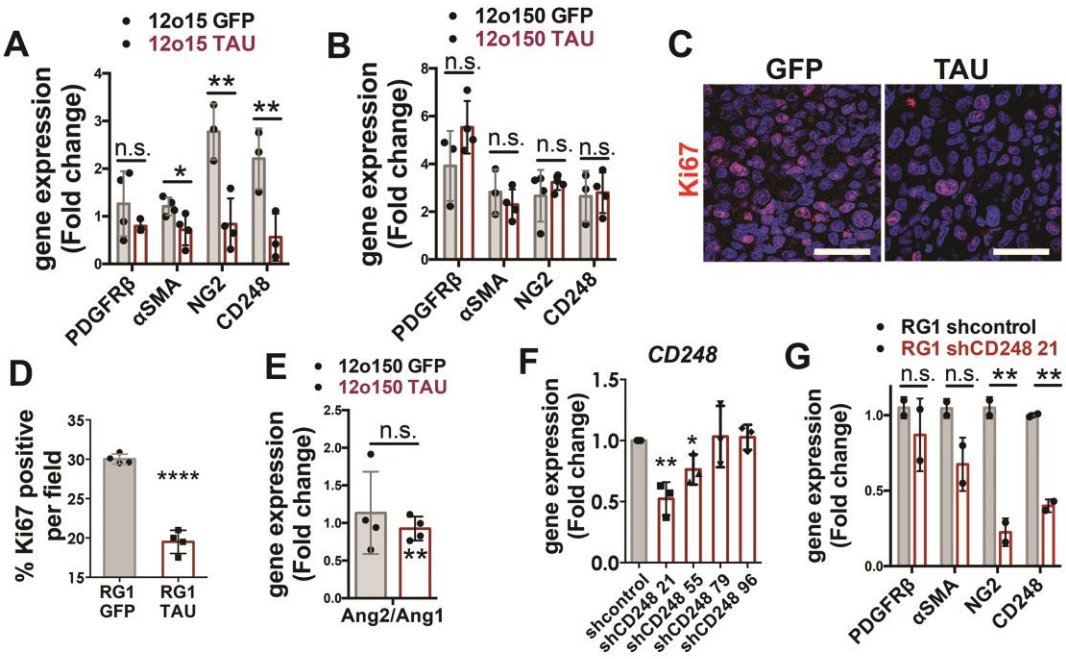

Fig. S8. Implication of the tumor-derived-pericytes on the glioma vasculature and growth. (**A** and **B**) qRT-PCR analysis of pericytic–related genes (using human-specific primers) in 12o15 (A) and 12o150 (B) xenografts expressing GFP or Tau (n=3 to 4). Mouse cDNA was used as a negative control. The expression of *HPRT* was used for normalization**.** (**C** and **D**) Representative images of Ki67 IF staining of sections from RG1 xenografts expressing GFP or Tau (C) and quantification of the number of Ki67 positive cells per field (D) (n=4). (**E**) Ratio of *Ang2/Ang1* expression measured by qRT-PCR in 12o150 tumors. The expression of HPRT was used for normalization (n=4). (**F**) qRT-PCR analysis of *CD248* levels after transduction of different shRNAs against the *CD248* gene in RG1 cells (n=3). The expression of *HPRT* was used for normalization. (**G**) qRT-PCR quantification of 4 pericyte markers: *CD248, NG2, αSMA* and *PDGFRβ*, after the transduction of shcontrol or shCD248 21 in the RG1 line (n=3). The expression of *HPRT* was used for normalization. Data shown as mean ± SD; Student's t test; *, $p \leq 0.05$; **, $p \leq 0.01$; ****, $p \leq 0.0001$, n.s. non significant. Scale bar 50 μm.

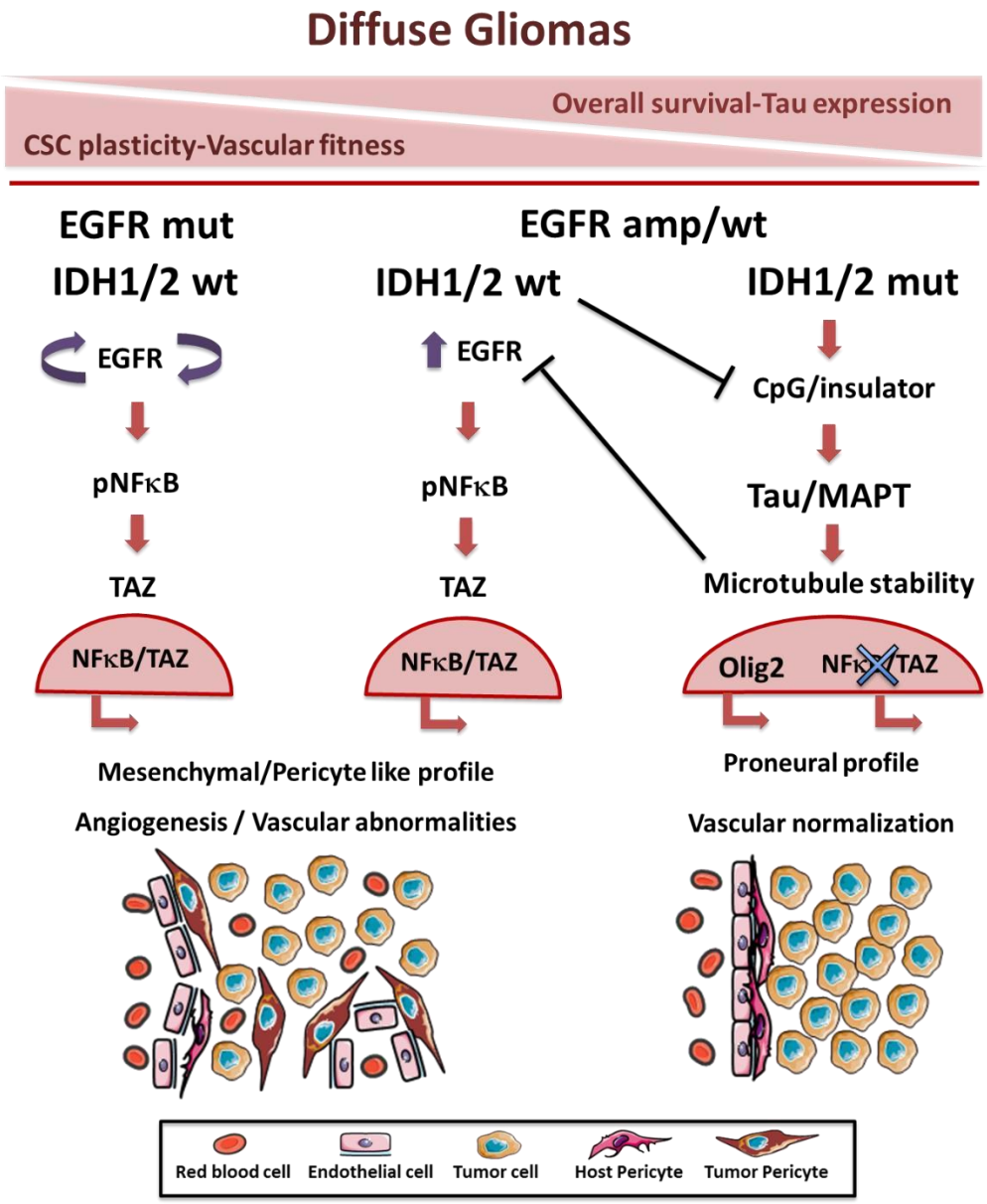

Fig. S9. Integrated stratification of diffuse gliomas based on the status of *EGFR* and *IDH* and the expression of Tau. EGFRmut and EGFRamp glioma cells generate pericytes (glioma-derived-pericytes, GDPs) with distinct vascular capacities. The GDPs are the master regulators of the vascular landscape, defining the leakiness of the BBB and the proliferative capacity of the tumors. In IDHmutant tumors, Tau expression is epigenetically induced and impairs the appearance of GDPs by inhibiting the EGFRamp-NF B-TAZ axis status.

Supplementary materials and methods.

DNA constructs and lentiviral/retroviral production

The lentivirus that encodes the longest wild type isoform of Tau in human brain harboring four repeats and two N-terminal inserts followed by GFP linked by an IRES was a gift from by Prof. Kenneth S. Kosik (UC Santa Barbara). As a control we used a lentivector encoding E-GFP, pRRLSIN.cPPT.PGK-GFP.WPRE (Addgene plasmid 12252). pLV-Hygro-Luciferase (VectorBuilder #VB150916-10098) was used as reporter. Lentiviral vector to express shRNAs were: shCD248 (Sigma #SHCLNG-NM_020404: TRCN0000053455, TRCN0000053457, TRCN00000443679, TRCN00000429396, TRCN0000043782) and shTAZ (TRCN0000370006, TRCN0000370007). Retroviral vectors used were pBabe-EGFR wt (#11011), MSCV-XZ066-GFP-EGFR vIII (#20737), pBabe-puro-Flag-IDH1 (#62923), pBabe-puro-Flag-IDH1-R132H (#62924) (Addgene) and pBabePuroTAZ-WT was a generous gift from Kun-Liang Guan. To obtain the virus, the 293T cells were transiently co-transfected with 5 μg of appropriate lentivector plasmid, 5 μg packaging plasmid pCMVdR8.74 (Addgene #Plasmid 22036) and 2 μg VSV-G envelope protein plasmid pMD2G (Addgene #Plasmid 12259) using Lipofectamine Plus reagent (Invitrogen). Retrovirus and lentivirus supernatant was prepared by transfection of 293T cells and collection of the supernatant 48 hr after.

Growth curve and sphere formation assay

Glioma cells were infected by the control lentivirus (LV-GFP) or lentivirus directing expression of TAU (LV-TAU-GFP). The tumor spheres were Accumax-dissociated to single cells, and 500/1000 cells of each condition were plated in a p24-well-plate in triplicate. Five days after plating, spheres and cell number were measured.

EGFR degradation experiment

GFP or TAU SVZ EGFRwt/amp cells were grown in stavirng media for 1h and then EGF (100 ng/ml) was added and the cells were incubated in the presence of DMSO, MG132 or Chloroquine for 2h. Then, cells were collected and lysed and subsequently analyzed by western blot, as described below.

Endothelial cell sprouting assay

In order to generate endothelial cell spheroids, $1x10^6$ cells of HMBEC were suspended in CM and seeded in nonadherent plates. These spheroids were harvest within 48 hours and embedded into matrigel in 96-well plates with conditioned medium generated for each cell line. After 24 h, sprouting was induced and the number of sprouts for each spheorid were quantified. For the generation of the conditioned media, RG1 (GFP or Tau) were grown during 48 hours in serum-free culture media (DMEM-F12 supplemented with FGF2 (50ng/ml) and penicillin-streptomycin). The medium was filtered with a 70-μm filter before use.

Intracraneal tumor formation and treatment in vivo

Animal experiments were reviewed and approved by the Research Ethics and Animal Welfare Committee at "Instituto de Salud Carlos III" (PROEX 244/14 and 02/16), in agreement with the European Union and national directives. Intracranial transplantation to establish orthotopic xeno- and allo-grafts was performed injecting 100.000-300.000 cells (resuspended in 2 μl of culture stem cell medium) with a Hamilton syringe into athymic Nude-Foxn1nu brains (Harlan Iberica). The injections were made into the striatum (coordinates: A–P, −0.5 mm; M–L, +2 mm, D–V, −3 mm; related to Bregma) using a Stoelting Stereotaxic device. When applicable, tumor growth was monitored in an IVIS equipment (Perkin Elmer) after intraperitoneal injection of D-luciferin (75 mg/Kg) (PerkinElmer). The animals were sacrificed at the onset of symptoms. Mice were treated with Epothilone D (Abcam, ab143616) (1 mg/kg two days per week through intra-peritoneal injection) and/or Temozolomide (Sigma Aldrich) (5mg/kg daily through intraperitoneal injection). Epothilone D was dissolved in 4% DMSO +10%Polysorbate. Temozolomide was dissolved in 1% BSA+PBS. Control animals were treated with these solvents.

In vivo limiting dilution assay

Increasin numbers of RG1 (GFP or TAU) cells were re-suspended in CM and Matrigel (BD) (1:10) and injected subcutaneously injected in nude mice. Animals were sacrificed before tumors reached a 1.5 cm in diameter. The statistical significances were calculated using the Extreme Limiting Dilution Analysis software (http://bioinf.wehi.edu.au/software/limdil/ index.html).

Inmunofluorescent (IF) and Inmunohistochemical (IHC) staining

Slides were heated at 60ºC for 1 hour followed by deparaffinization and hydration, washed with water, placed into antigen retrieval solution (pressure cooking) in 10 mM sodium citrate pH 6.0. Paraffin sections were permeabilized with 1% Triton X-100 (Sigma-Aldrich) in PBS and blocked for 1 hour in PBS with 5% BSA (Sigma), 10% FBS (Sigma) and 0,1% Triton X-100 (Sigma). The following primary antibodies (Table S4) were incubated O/N at 4ºC. The second day, sections were washed with PBS three times prior to incubation with the appropriate secondary antibody (Table S4) (1:200 dilution) for 2h at room temperature. Prior to coverslip application, nuclei were counterstained with DAPI and imaging was done with Leica SP-5 confocal microscope. Otherwise, IHC sections were incubated with biotinylated secondary antibodies (1:200 dilution). Target proteins were detected with the ABC Kit and the DAB kit (Vector Laboratories).

IHC quantification

The IHC score was judged from 0 (no staining) to 3 (Tau staining) or 4 (CD248 staining) on those samples with the strongest positive staining. For the longitudinal analysis of the primary and relapsed tumors we calculated the score of 10 high magnification pictures of each sample. The data depicted in Figure 2 E and F is the average of these 10 pictures. For the quantification of the vasculature, we counted the number of dilated vessels per high-magnification field.

Western Blot analysis

Protein content was quantified using BCA Protein Assay Kit (Thermo-Fisher-Scientific). Approximately 20 µg of proteins were resolved by 10% or 12% SDS-PAGE and they were then transferred to a nitro cellulose membrane (Hybond-ECL, Amersham Biosciences). The membranes were blocked for 1 h at room temperature in TBS-T (10 mM Tris-HCl [pH 7.5], 100 mM NaCl, and 0.1% Tween-20) with 5% skimmed milk, and then incubated overnight at 4ºC with the corresponding primary antibody diluted in TBS-T. The primary antibodies and the dilutions are shown in Table S4. After washing 3 times with TBS-T, the membranes were incubated for 2 h at room temperature with their corresponding secondary antibody (HRP-conjugated anti mouse or anti rabbit, DAKO) diluted in TBS-T. Proteins were visible by enhanced chemiluminiscence with ECL (Pierce) using the Amersham Imager 680.

qRT-PCR assay

RNA was extracted from the tissue using RNA isolation Kit (Roche). Total RNA (1µg) was reverse transcribed with PrimeScript RT Reagent Kit (Takara). Quantitative real-time PCR was performed using the Light Cycler 1.5 (Roche) with the SYBR Premix Ex Taq

(Takara). The primers used for each reaction are indicated in Table S5. Gene expression was quantified by the delta-delta Ct method.

EGFR Sequencing of primary GBMs

To identify point EGFR mutations, cDNAs from the different cell lines were sequenced using the primers indicated in Table S6. The sequences were aligned and collated with the EGFR transcript (NM_005228.4) in the NIH GenBank database using the multiple sequence alignment tool Clustal Omega (www.ebi.ac.uk/Tools/msa/clustalo/) and the Sequencing Analysis Software v5.3.1 from Applied Biosystems. The identified mutations were analyzed at cBioPortal (www.cbioportal.org).

Gene expression and survival analyses

Tau (MAPT) gene expression and follow-up overall survival data from human glioma tumors corresponding to TCGA Glioblastoma (GBM) and Brain lower grade Glioma (LGG) data sets were downloaded respectively from cBioPortal (http://www.cbioportal.org/) and TCGA databases (http://tcga-data.nci.nhi.gov/docs/publications/lgggbm_2015) using UCSC cancer browser. Kaplan-Meier survival curves were done within TCGA-GBM, TCGA-LGG, TCGA-GBM-LGG, Rembrandt, Gravendeel, Ducray, Freije and Nutt cohorts upon stratification based into low and high groups using expression values from *Tau (MAPT)* gene. Significance of differences in survival between groups was calculated using the log-rank test. These data were obtained from UCSC Xena-Browser (https://xenabrowser.net) and Gliovis (http://gliovis.bioinfo.cnio.es). Classification into classical, mesenchymal, neural and proneural subtypes was retrieved from the TCGA GBM data set (https://www.ncbi.nlm.nih.gov/pubmed/24120142) together with Tau/MAPT expression values. Differences in Tau expression between mesenchymal and other groups were calculated using Student's t-test. In David gene onotology analysis we have used a cluster of 1000 genes co-expressed with Tau/MAPT. They were chosen using the highest values of the Spearman´s correlations. Correlation between gene expression values of MAPT versus other genes was done using Pearson analysis. Gene Set Enrichment Analysis (GSEA) was computed into the TCGA-GBMLGG cohort (RNAseq (IlluminaHiSeq)) using Tau gene expression as a continuous class label and genesets from the "CGP: chemical and genetic perturbations" and "CP:BIOCARTA: BioCarta gene sets" (n=) from the MSigDB genesets database.

Analysis of methylation of the MAPT gene and CTCF Chip-seq binding

DNA-methylation analysis in human glioma within the MAPT locus was done using the TCGA data (Illumina Infinium HumanMethylation450 platform). Methylation beta values from 56 probes within MAPT locus were retrieved from the Xena browser (https://xenabrowser.net/) together with MAPT gene expression values. Pearson correlation values between each methylation probe and gene expression values, calculated for all samples, was calculated and represented together with the CpG islands located at the MAPT locus (CpG302, CpG26 and CpG21). Both TCGA LGG-GBM and LGG cohorts were individually analyzed. Correlation values were independently calculated for IDH1 mutant or wild-type samples in the TCGA LGG cohort. ChIP-seq analysis using anti-CTCF antibody was performed from profiling in IDH1 mutant and wild-type glioma patient specimens and culture models (GSE70991). Briefly tdf files from GEO repository from both IDH1 mutant and wild-type samples were downloaded and visualized using IGV browser. CTCF occupancy at the CpG islands located from MAPT loci was visualized.

Supplementary Table 1. Human samples

Sample	Hospital	Diagnosis	Grade	Tau IHC	IDH	ATRX
1	H12O	Glioblastoma	IV	0	wt	wt
2	H12O	Glioblastoma	IV	0	wt	wt
3	H12O	Glioblastoma	IV	1	wt	wt
4	H12O	Glioblastoma	IV	0	wt	wt
5	H12O	Glioblastoma	IV	0	wt	wt
6	H12O	Glioblastoma	IV	2	wt	wt
7	H12O	Glioblastoma	IV	3	wt	wt
8	H12O	Glioblastoma	IV	3	wt	wt
9	H12O	Glioblastoma	IV	1	wt	wt
10	H12O	Glioblastoma	IV	1	wt	wt
11	H12O	Glioblastoma	IV	0	wt	wt
12	H12O	Anaplastic Astrocytoma	nd	3	mut	wt
13	H12O	Glioblastoma	IV	1	wt	wt
14	H12O	Glioblastoma	IV	0	wt	mut
15	H12O	Glioblastoma	IV	1	wt	mut
16	H12O	Glioblastoma	IV	2	wt	wt
17	H12O	Glioblastoma	IV	3	wt	wt
18	H12O	Glioblastoma	IV	2	wt	mut
19	H12O	Glioblastoma	IV	0	wt	wt
20	H12O	Glioblastoma	IV	0	wt	wt
21	H12O	Glioblastoma	IV	1	wt	wt
22	H12O	Glioblastoma	IV	0	wt	wt
23	H12O	Glioblastoma	IV	1	wt	wt
24	H12O	Glioblastoma	IV	0	wt	wt
25	H12O	Glioblastoma	IV	1	wt	mut
26	H12O	Glioblastoma	IV	3	wt	wt
27	H12O	Glioblastoma	IV	1	wt	wt
28	H12O	Glioblastoma	IV	0	wt	wt
29	H12O	Glioblastoma	IV	0	wt	wt
30	H12O	Glioblastoma	IV	1	wt	wt
31	H12O	Glioblastoma	IV	1	wt	wt
32	H12O	Glioblastoma	IV	0	wt	wt
33	H12O	Glioblastoma	IV	0	wt	wt
34	H12O	Oligodendroglioma	nd	1	mut	wt
35	H12O	Oligodendroglioma	III	2	mut	wt
36	H12O	Diffuse mindline glioma	nd	2	wt	mut
37	H12O	Anaplastic Astrocytoma	III	0	wt	wt
38	H12O	Astrocytoma	II	1	wt	nd
39	H12O	Anaplastic Astrocytoma	III	3	mut	mut
40	H12O	Anaplastic Astrocytoma	III	3	mut	mut
41	H12O	Diffuse Astrocytoma	II	3	mut	mut

42	H12O	Anaplastic Astrocytoma	III	3	wt	mut
43	H12O	Diffuse Astrocytoma	II	3	wt	wt
44	H12O	Anaplastic Astrocytoma	III	1	mut	mut
45	H12O	Anaplastic Astrocytoma	III	2	mut	nd
46	H12O	Anaplastic Astrocytoma	III	3	wt	wt
47	H12O	Anaplastic Astrocytoma	III	2	mut	mut
48	H12O	Anaplastic Astrocytoma	III	3	wt	wt
49	H12O	Anaplastic Astrocytoma	III	0	mut	nd
50	H12O	Astrocytoma	II	2	mut	nd
51	H12O	Anaplastic Astrocytoma	III	3	wt	mut
52	H12O	Glioblastoma	IV	3	mut	mut
53	H12O	Astrocytoma	II	2	mut	mut
54	H12O	Anaplastic Astrocytoma	III	3	mut	mut
55	H12O	Anaplastic Astrocytoma	III	1	wt	wt
56	H12O	Anaplastic Astrocytoma	III	0	mut	mut
57	H12O	Anaplastic Astrocytoma	III	3	mut	mut
58	H12O	Anaplastic Astrocytoma	III	3	mut	nd
59	H12O	Anaplastic Astrocytoma	III	3	mut	nd
60	H12O	Anaplastic Astrocytoma	III	1	mut	mut
61	H12O	Anaplastic Astrocytoma	III	2	mut	mut
62	H12O	Astrocytoma	II	3	mut	mut
63	H12O	Diffuse Astrocytoma	II	2	mut	mut
64	H12O	Anaplastic Astrocytoma	III	3	mut	mut
65	H12O	Astrocytoma	II	2	wt	nd
66	H12O	Diffuse Astrocytoma	II	3	mut	mut
67	H12O	Anaplastic Astrocytoma	III	1	mut	mut
68	H12O	Anaplastic Astrocytoma	III	1	wt	nd
69	H12O	Anaplastic Astrocytoma	III	3	wt	nd
70	La Fe	Glioblastoma	IV	0	nd	nd
71	La Fe	Glioblastoma	IV	0	nd	nd
72	La Fe	Glioblastoma	IV	0	nd	nd
73	La Fe	Glioblastoma	IV	0	nd	nd
74	La Fe	Glioblastoma	IV	0	nd	nd
75	La Fe	Glioblastoma	IV	0	nd	nd
76	La Fe	Glioblastoma	IV	0	nd	nd
77	La Fe	Glioblastoma	IV	0	nd	nd
78	La Fe	Glioblastoma	IV	0	nd	nd
79	La Fe	Glioblastoma	IV	0	nd	nd

80	La Fe	Glioblastoma	IV	0	nd	nd
81	La Fe	Oligodendroglioma	nd	1	nd	nd
82	La Fe	Glioblastoma	IV	2	nd	nd
83	HGM	Glioblastoma	IV	1	nd	nd
84	HGM	Oligoastrocytoma	II	2	mut	nd
85	HGM	Oligodendroglioma	II	3	mut	nd
86	La Fe	Glioblastoma	IV	0	nd	nd
87	La Fe	Glioblastoma	IV	2	nd	nd
88	La Fe	Glioblastoma	IV	1	nd	nd
89	La Fe	Glioblastoma	IV	0	nd	nd
90	La Fe	Glioblastoma	IV	0	nd	nd
91	La Fe	Glioblastoma	IV	0	nd	nd
92	La Fe	Anaplastic Oligoastrocytoma	III	2	nd	nd
93	La Fe	Anaplastic Oligoastrocytoma	III	3	mut	nd
94	La Fe	Diffuse Glioma	II	3	mut	nd
95	La Fe	Glioblastoma	IV	2	wt	nd
96	La Fe	Glioblastoma	IV	0	wt	nd
97	La Fe	Glioma difuso anaplásico, de fenotipo astrocitario	III	2	mut	nd
98	La Fe	Glioma difuso anaplásico, de fenotipo astrocitario	III	2	mut	mut
99	La Fe	Glioblastoma	IV	2	wt	nd
100	La Fe	Glioma difuso de fenotipo oligodendroglial	II	1	mut	wt
101	La Fe	Oligodendroglioma	II	1	mut	wt
102	La Fe	Glioblastoma	IV	2	wt	wt

Supplementary Table 2. Paired human samples

Sample	Hospital	Year of surgery	Progression Free Survival	Diagnosis	Grade	Tau IHC	IDH	ATRX
3	H12O	2010		Astrocytoma	III	2.6	mut	mut
	H12O	2011	18 months	Astrocytoma	III	1.6	mut	mut
5	H12O	2009		Astrocytoma	II	2.3	mut	mut
	H12O	2011	22 months	Glioblastoma	IV	0.7	mut	mut
6	H12O	2008		Oligodendroglioma	III	1.6	mut	wt
	H12O	2011	29 months	Oligodendroglioma	III	1.5	mut	wt
7	H12O	2014		Astrocytoma	II	1.2	mut	mut
	H12O	2016	19 months	Glioblastoma	IV	0.2	mut	mut
8	H12O	2013		Astrocytoma	II	1.7	mut	mut
	H12O	2018	50 months	Astrocytoma	III	0.8	mut	mut
10	H12O	2010		Astrocytoma	II	1.2	mut	mut
	H12O	2018	100 months	Astrocytoma	II	1.7	mut	mut
11	H12O	2012		Astrocytoma	III	1.2	mut	mut
	H12O	2015	39 months	Glioblastoma	IV	0.0	mut	mut
13	H12O	2013		Astrocytoma	II	1.5	mut	mut
	H12O	2016	42 months	Astrocytoma	II	2.6	mut	mut

Supplementary Table 3. GB cell lines. (nd: not diagnosed. 0: wild type. 1: altered)

Cell line	Origin	EGFR amp	EGFR mut	PTEN loss	p53 mutation
RG1	Mazzoleni et al.	1	0	0	1
12o01	Hospital 12 de Octubre	1	1 (vIII)	0	1
12o02	Hospital 12 de Octubre	0	0	1	1
12o12	Hospital 12 de Octubre	1	1(vIII)	nd	0
12o15	Hospital 12 de Octubre	0	0	0	1
12o16	Hospital 12 de Octubre	0	mut	nd	nd
12o22	Hospital 12 de Octubre	1	1(vIII)	nd	nd
12o29	Hospital 12 de Octubre	nd	nd	nd	nd
12o33	Hospital 12 de octubre	1	nd	nd	nd
12o40	Hospital 12 de octubre	nd	nd	nd	nd
12o43	Hospital 12 de Octubre	nd	nd	nd	nd
12o44	Hospital 12 de Octubre	nd	nd	nd	nd
12o49	Hospital 12 de Octubre	1	1 (vII)	nd	nd
12o53	Hospital 12 de Octubre	nd	nd	nd	nd
12o56	Hospital 12 de Octubre	nd	nd	nd	nd
12o84	Hospital 12 de Octubre	1	1 C.1118C>A	0	0
12o89	Hospital 12 de Octubre	0	1 V774M	mut	1
12o107	Hospital 12 de Octubre	0	0	0	1
12o108	Hospital 12 de Octubre	0	0	0	0
12o113	Hospital 12 de Octubre	1	0	0	0
12o116	Hospital 12 de Octubre	nd	nd	nd	Nd
12o121	Hospital 12 de Octubre	1	0	1	0
12o124	Hospital 12 de Octubre	1	nd	nd	nd
12o126	Hospital 12 de Octubre	0 1	1 G1134S	1	1
12o129	Hospital 12 de Octubre	Nd	nd	nd	nd
12o150	Hospital 12 de Octubre	0	1 L760P/M945I	mut	1
GB4	Hospital Ramón y Cajal	nd	nd	Nd	1
GB19	Hospital Ramón y Cajal	nd	nd	nd	1

Supplemetary Table 4. Antibodies

Antibody	Dilution	Source
Acetyl-Tubulin	1:5000 (WB)	Sigma
AKT	1:1000 (WB)	Cell Signaling (4691)
ANGPT2	1:100(IF)	Santa Cruz Biotechnology (SC-74403)
α SMA	1:500 (WB) 1:100 (IHC)	Santa Cruz Biotechnology (SC-32251)
β-Actin	1:1000 (WB)	Sigma
β-catenin	1:1000 (WB)	Cell
BrdU	1:100 (IHC)	Dako
CD248	1:500 (WB)	Santa Cruz Biotechnology (SC-377221)
EGFR	1:1000 (WB)	Cell Signaling (2232)
Endomucin	1:100 (IF)	Santa Cruz Biotechnology (SC-65495)
GAPDH	1:500 (WB)	Santa Cruz Biotechnology (SC-47724)
GFP	1:100(IHC)	Santa Cruz Biotechnology
NG2		
OLIG2	1:100(IHC)	Santa Cruz Biotechnology
phospho-Ser431 AKT	1:1000 (WB)	Cell Signaling (4549)
phospho-Tyr751 PDGFRB	1:1000 (WB)	Cell Signaling (4549)
phospho-Tyr740 PDGFRB	1:100 (IHC)	SIGMA (SAB4504202)
PDGFRB	1:1000 (WB)	Cell Signaling (4564)
phospo-Tyr1068 EGFR	1:1000 (WB)	Cell Signailing (3777)
phospo-Ser536 NFK β	1:1000 (WB)	Cell Signaling (3033)
TAU 7.51	1:500 (WB)	
TAU-5	1:500	Calbiochem (577801)
TAU-12	1:500	Millipore (MAB2241)
TAU	(IHQ)	Dako
YAP-TAZ	1:1000 (WB) 1:50 (IHC)	Cell Signaling SIGMA

anti mouse -Dylight 488	1:500 (IF)	Jackon Immunoresearch
anti rabbit -Dylight 488	1:500 (IF)	Jackon Immunoresearch
Anti mouse-Cy3	1:500 (IF)	Jackon Immunoresearch
Anti rabbit-Cy3	1:500 (IF)	Jackon Immunoresearch
Anti rat-Cy5	1:500 (IF)	Jackon Immunoresearch

Supplementary Table 5. qRT-PCR primers

Specie	gene	Forward (5'-3´)	Reverse (3'-5´)
mouse	CD31	TCCAGGTGTGCGAAATGCT	TGGCAGCTGATGCCTATGG
mouse	ENG	TGCACTTGGCCTACGACTC	TGGAGGTAAGGGATGGTAGCA
mouse	VE-CAD	TTACTCAATCCACATACACATTTTCG	GCATGATGCTGTACTTGGTCATC
mouse	CD248	TTGATGGCACCTGGACAGAGGA	TCCAGGTGCAATCTCTGAGGCT
mouse	αSMA	ACCATCGGCAATGAGCGTTTCC	GCTGTTGTAGGTGGTCTCATGG
mouse	PDGFRB	CCGGAACAAACACACCTTCT	TATCCATGTAGCCACCGTCA
mouse	MMP9	GCAAGGGGCCGTGTCTGGAGATTC	GCCCACGTCGTCCACCTGGTT
mouse	LMNA	TTGCCTCAACTGCAATGACAA	TCTCGATGTCGGTAAAACCCC
mouse	KDR	TTTGGCAAATACAACCCTTCAGA	GCAGAAGATACTGTCACCACC
mouse	VEGFR2	CATCACCGAGAACAAGAACAAAACT	GATACCTAGCGCAAAGAGACACATT
mouse	TEK	ACGGACCATGAAGATGCGTCAACA	TCACATCTCCGAACAATCAGCCTGG
mouse	NRP1	GCTTGTGCTCTATGCAGATCG	TCGACGAACTCCTGGTGATTTA
mouse	EPHA2	GCACAGGGAAAGGAAGTTGTT	CATGTAGATAGGCATGTCGTCC
mouse	AQP1	AGGCTTCAATTACCCACTGGA	GTGAGCACCGCTGATGTGA
mouse	VEGF A	TGCCAAGTGGTCCCAGGCTGC	CCTGCACAGCGCATCAGCGG
mouse	PDGF A	GATACCTCGCCCATGTTCTG	CAGGCTGGTGTCCAAAGAAT
mouse	PDGF B	GGGCCCGGAGTCGGCATGAA	AGCTCAGCCCCATCTTCATCTTACGG
mouse	PGF	GAGGCCAGAAAGTCAGGGGGC	ATGGGCCGACAGTAGCTGCGA
mouse	CCL2	AGGTCCCCTGTCATGCTTCTG	TCTCCAGCCTACTCATTGGG
mouse	PI3KCG	GCTCTTCGCCAATCACACAAAC	GGCATTCCTGTCATCAGCATC
mouse	NG2	GACGGCGCACACACTTCTC	TGTTGTGATGGGCTTGTCAT
mouse	Ang1	CATTCTTCGCTGCCATTCTG	GCACATTGCCCATGTTGAATC
mouse	Ang2	TTAGCACAAAGGATTCGGACAAT	TTTTGTGGGTAGTACTGTCCATTCA
human	MAPT	GTCGAAGATTGGGTCCCTGG	GACACCACTGGCGACTTGTA
human	αSMA	TAGCACCCAGCACCATGAAGATCA	GAAGCATTTGCGGTGGACAATGGA
human	NG2	AGCTCTACTCTGGACGCC	ATCGACTGACAACGTGGC
human	CD248	AGACCACCACTCATTTGCCTGGAA	AGTTGGGATAATGGGAAGCGTGGT
human	PDGFRB	ACGGCTCTACATCTTTGTGCCAGA	TCGGCATGGAATGGTGATCTCAGT
human	SNAIL 1	ACCACTATGCCGCGCTCTT	GGTCGTAGGGCTGCTGGAA
human	SNAIL 2	ATCTGCGGCAAGGCGTTTTCCA	GAGCCCTCAGATTTGACCTGTC
human	ZEB 1	GGCATACACCTACTCAATACGG	TGGGCGGTGTAGAATCAGAGTC
human	ZEB 2	AATGCACAGAGTGTGGCAAGGC	CTGCTGATGTGCGAACTGTAGC
human	TWIST 1	CCGGAGACCTAGATGTCATTG	CACGCCCTGTTTCTTTGAAT
human	SERPINE	CATAGTGGAAGTGATAGAT	ACTCTGTTAATTCGTCTT
human	TAZ	TTTCCTCAATGGAGGGCCA	GGGTGTTTGTCCTGCGTTTT
human	CD133	GCCACCGCTCTAGATACTGC	TGTTGTGATGGGCTTGTCAT
human	SOX2	GCGAACCATCTCTGTGGTC	AATGGAAAGTTGGGATCGAA
human	L1 CAM	TCGCCCTATGTCCACTACACCT	ATCCACAGGGTTCTTCTCTGGG
human	DLL3	AAACCTATGGGCTTGAGGAG	CGCTGAGTACAATCAGTGGAA
human	REST	CGGCTAACAATACTAATCG	TAGACTCGCTCATTATCC
human	LIF	CATGAACCAGATCAGGAG	GCTGTGTAATAGAGAATAAAGAG
human	NESTIN	GCGGCTGCGGGCTACTGAAA	CCAGCTGCTGCCGACCTTCC
human	OLIG2	CGGCTTTCCTCTATTTTGGTT	GTTACACGGCAGACGCTACA

Supplementary Table 6. Sequencing primers

Species	Gene name	Forward (5'-3´)	Reverse (3'-5´)
human	**EGFR**	CAGTATTGATCGGGAGAG	CATCTCATAGCTGTCGGC
		CAACATGTCGATGGACTTCCA	TTCGCATGAAGAGGCCGATC
		GCCCCCACTGCGTCAAGACC	AGCTTTGCAGCCCATTTCTA-
		CAGCGCTACCTTGTCATTCA	CTATCCTCCGTGGTCATGCT